TECHNISCHE UNIVERSITÄT WIEN
Vienna University of Technology

The Mass-Imbalanced Hubbard Model in Infinite Dimensions

Or: How Fermi Liquids Get Dirty

supervised by
Prof. Ph.D. Karsten Held

co-supervised by
M.Sc. Markus Wallerberger

written by
Marie-Therese Philipp
Matric.no. 1226010
marie.therese1@gmx.de

Vienna, December 21, 2015

Abstract

The description of strongly correlated electron systems is of great interest within the field of solid state physics. One of the most successful approaches is mapping the full problem onto the Hubbard model, and treating it within dynamical mean field theory. Here the lattice model—with nearest neighbor hopping and screened, short-range Coulomb potential—is mapped onto a single-site quantum impurity problem and subsequently iterated in a self-consistency loop until convergence is reached. On the one hand it can be tackled by a computationally expensive impurity solver. In the scope of this work, w2dynamics is used elaborating a continuous time quantum Monte Carlo integration.

On the other hand it can be tackled by a simplification of the Hubbard model such as is represented by the Falicov-Kimball model in the sense that one spin gets frozen. It allows for a short-cut in the self-consistency loop since the impurity problem becomes trivial to solve. It naturally changes the physics described by the system fundamentally. However the connection to the Hubbard model is not well understood. Investigating the transition of the Hubbard model to the Falicov-Kimball model is of great interest as one can easily imagine the case of spin-dependent mobility in a real system, such as half metals. Experimentally it can be simulated by loading ultra-cold fermions of different masses in an optical lattice as current research in the group around T. Esslinger shows. In the scope of this thesis the phase space spanned by the Hubbard model on one side and the Falicov-Kimball model on the other, known as mass-imbalance, is analyzed focusing on the Mott transition on the Bethe lattice in infinite dimensions. It is a paramagnetic metal insulator transition at low temperatures driven by the interaction strength featuring a first order transition with coexistence region in case of the Hubbard model and a crossover in case of the Falicov-Kimball model.

In Chapter 1 the basic theoretical understanding of strongly correlated electron systems and its limits is established. It further introduces the Hubbard model, the Falicov-Kimball model as well as the Anderson impurity problem. Subsequently the properties of the Bethe lattice and the Mott transition are discussed.

Chapter 2 firstly describes the code used to solve the Falicov-Kimball model and secondly the code added to the preexisting w2dynamics in order to slowly freeze one spin.

In Chapter 3 we engage in a discussion on the results. One particle quantities are presented with a special focus on the imaginary part of the self-energy in Matsubara frequencies, the occupancy of a site as well as the spectral function.

Chapter 4 reviews the presented work giving an overview and outlook to what we presently do or do not understand about the transition of the Hubbard model to the Falicov-Kimbal model at half filling on the Bethe lattice in infinite dimensions.

Thanks Markus for introducing me to this wonderful group!

During research I was not only strongly supported by my co-supervisor and mentor Markus Wallerberger, but also by his former diploma student and now Ph.D. student Patrik Gunacker. Many fruitful discussions have been held with Ciro Taranto, Tin Ribic, Alessandro Toschi, Benedikt Hartl and Thomas Schäfer.

Contents

1 Introduction

1.1 Strongly correlated systems

In the quantum theory of many-body systems "many" refers to something of the order of 10^{23} particles. Since the three-body problem is already insolvable it is apparent that good strategies are needed to describe these systems. In thermodynamics, statistical methods are used to arrive at a description based on macroscopic observables, which has to be consistent with microscopic physical laws. (**?**)

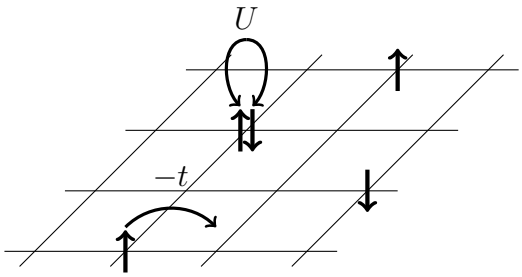

Figure 1.1: Hubbard model: At each lattice site one considers Coulomb repulsion U between two electrons. Electrons move according to the hopping amplitude $-t$ in correspondents to the kinetic energy.

An approach to describe a system of many particles from a microscopical point of view is by means of a *lattice model*. The *Hubbard model* is a lattice model with *nearest-neighbor* (NN) hopping and Coulomb interaction, which manifests itself as the Pauli exclusion principle and the Hubbard U, on each lattice site. This is expressed by the Hubbard Hamiltonian:

$$\mathcal{H}_{\text{Hub}} = -t \sum_{<i,j>} \sum_{\sigma=\uparrow,\downarrow} \left[\hat{c}^{\dagger}_{i\sigma} \hat{c}_{j\sigma} + \hat{c}^{\dagger}_{j\sigma} \hat{c}_{i\sigma} \right] + U \sum_{i} \left(\hat{c}^{\dagger}_{i\uparrow} \hat{c}^{\dagger}_{i\downarrow} \hat{c}_{i\downarrow} \hat{c}_{i\uparrow} \right) - \mu \sum_{i} \sum_{\sigma=\uparrow,\downarrow} \left(\hat{c}^{\dagger}_{i\sigma} \hat{c}_{i\sigma} \right), \quad (1.1)$$

where μ is the chemical potential and $\hat{c}^{\dagger}_{i\sigma}$ and $\hat{c}_{i\sigma}$ are the creation and annihilation field operators for the spin σ on the lattice site i. The first term is called hopping term as it expresses the kinetic energy of the electrons and thus their mobility by the NN hopping amplitude $-t$. The summation is over NN sites $< i, j >$ and spins σ. The second term is referred to as Coulomb interaction term. It describes the energy U the system has to pay, if two electrons occupy the same site. (**?**)

In Fig. **??** we see an example of a lattice, where spin up and spin down electrons (shown as arrows pointing upwards and downwards) are moving on a two-dimensional square lattice.

Even though in this model only NN interaction is considered, we are still left with a complex system to solve. The Hubbard U dependency of the Hamiltonian $\mathcal{H}_{\text{Hub}}$ causes the operator not to be diagonal in momentum space. If the Coulomb interaction term is neglected, the limit of free electron gas is described. In the model of free electron

gas the system is reduced to an effective one-body problem by looking at one electron and averaging over the rest of the system. This problem can in principle be solved with the appropriate boundary conditions as known from basic quantum theory. However neglecting the Coulomb interaction term only holds as long as the strength of the effective particle-particle interaction within the system is well below the kinetic energy, which manifests itself as the hopping amplitude $-t$. Strong electron correlation is predominant in systems with partially filled 3d or 4f orbitals due to relatively strong localization of the radial wave function. In these *strongly correlated systems* the propagation of an electron cannot be approximated by neglecting the Coulomb interaction term and thus the model of a free electron gas is not applicable. (**?**)

Furthermore the hopping amplitude $-t$ dependency of the Hamiltonian $\mathcal{H}_{\text{Hub}}$ causes the operator not to be diagonal in real coordinate space either.

The description of strongly correlated electron systems thus requires approximate techniques such as the *dynamical mean field theory* (DMFT). DMFT tackles the problem by mapping a lattice model onto a *single-site quantum impurity problem* in a self-consistent manner. It takes local quantum fluctuations (e.g. temporal fluctuations between possible quantum states) fully into account and freezes spatial fluctuations. (**?**)

The single-site *Anderson impurity model* (AIM) describes an impurity site, on which the Coulomb interaction is considered, hybridizing with an external bath of non-interacting fermions. It is described by the Hamiltonian

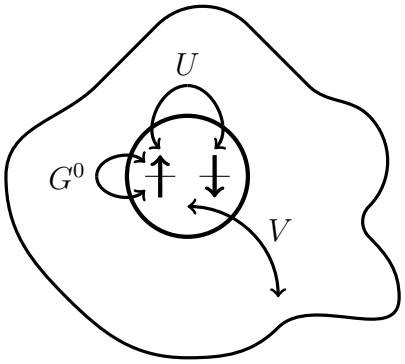

Figure 1.2: Impurity model: On the impurity site the Coulomb interaction between two electrons is considered. The impurity interacts with the external bath—formed by averaging over the rest of the system—via the hybridization V.

$$\mathcal{H}_{\text{AIM}} = \sum_{l,\sigma} \left[V_{l,\sigma}\, \hat{a}^\dagger_{l\sigma} \hat{c}_\sigma + V^*_{l,\sigma}\, \hat{c}^\dagger_\sigma \hat{a}_{l\sigma} \right] + U \left(\hat{c}^\dagger_\uparrow \hat{c}^\dagger_\downarrow \hat{c}_\downarrow \hat{c}_\uparrow \right) + \sum_{l,\sigma} \epsilon_l \hat{a}^\dagger_{l\sigma} \hat{a}_{l\sigma} - \mu \left(\hat{c}^\dagger_\uparrow \hat{c}_\uparrow + \hat{c}^\dagger_\downarrow \hat{c}_\downarrow \right) \quad (1.2)$$

where $\hat{c}^\dagger_\sigma$ and $\hat{c}_\sigma$ are the creation and annihilation field operators for the spin $\sigma = \uparrow, \downarrow$ on the impurity site, $\hat{a}^\dagger_{l\sigma}$ and $\hat{a}_{l\sigma}$ are the creation and annihilation field operators for the spin σ of a bath electron, ϵ_l is the effective energy of a bath electron and V_l is the hybridization strength. (**?**)

In Fig. **??** we see a scheme of an impurity site embedded in an effective medium. The impurity is connected with the external bath via the hybridization V. These dynamics can be described using Green's functions. The bare Green's function $G^0(\tau - \tau')$ is a propagator referring to the effective amplitude for an electron to be created on the

impurity site at time τ—coming from the external bath— and to be annihilated at time τ'—going back to the external bath—, when no interaction U is present on the impurity.

1.1.1 Atomic limit

In order to gain a better understanding of the AIM it is instructive to look at the *atomic limit*, where the hybridization $V_{l,\sigma}$ equals zero. It enables the separation of the Hamiltonian $\mathcal{H}_{\mathrm{AIM}}$ in Eq. (**??**) into a local part, describing the impurity site, and a bath Hamiltonian,

$$V_{l,\sigma} = 0 : \mathcal{H}_{\mathrm{AIM}} = \mathcal{H}^{\mathrm{imp}}_{\mathrm{AIM}} + \mathcal{H}^{\mathrm{bath}}_{\mathrm{AIM}}. \quad (1.3)$$

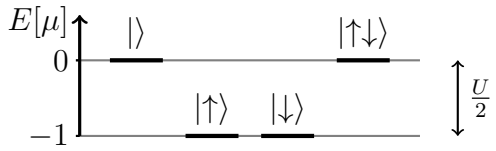

Figure 1.3: Eigenenergies of the four possible states of occupation of the impurity site at half filling in the limit $T \to 0$

Therefore we obtain the local Hamiltonian

$$\mathcal{H}^{\mathrm{imp}}_{\mathrm{AIM}} = U(\hat{c}^\dagger_\uparrow \hat{c}^\dagger_\downarrow \hat{c}_\downarrow \hat{c}_\uparrow) - \mu \left(\hat{c}^\dagger_\uparrow \hat{c}_\uparrow + \hat{c}^\dagger_\downarrow \hat{c}_\downarrow \right). \quad (1.4)$$

The Hamiltonian $\left(\mathcal{H}^{\mathrm{imp}}_{\mathrm{AIM}}\right)^{\{|s\rangle\}}$ is diagonal in the basis

$$\{|s\rangle\} = \{|\rangle, |\uparrow\rangle, |\downarrow\rangle, |\uparrow\downarrow\rangle\} \quad (1.5)$$

spanned by the four possible states of occupation of the impurity site. Solving for the eigenenergies yields

$$E_{\{|s\rangle\}} = \{0, -\mu, -\mu, U - 2\mu\}. \quad (1.6)$$

Half filling refers to the case $\mu = U/2$ and thus at the limit temperature $T \to 0$ the system's ground state has densities $n_\uparrow = n_\downarrow = 0.5$ as shown in Fig. **??**.

1.1.2 Validity of the DMFT approximation

DMFT implies correlations to be local. This assumption may be presumptuous considering Newton's cradle. The force of one ball being lifted and released is transmitted to the other end having clearly a non local effect in this two-dimensional system. However in the limit of large spatial dimensions $d \to \infty$ DMFT is exact. (**?**) In the case $d = 3$ DMFT still gives meaningful results. However, it fails in systems with strong non-local correlation, such as lower-dimensional lattices and systems close to a second-order phase transition.

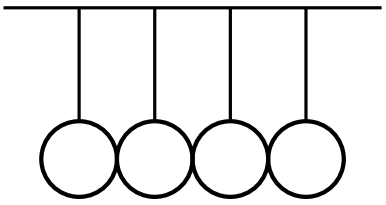

Figure 1.4: Newton's cradle as an example of non-local correlation in a two-dimensional system

1.1.3 Propagation

The dynamics of a system of many particles are described by many-body propagators. The one-particle propagator is of the form,

$$K(\boldsymbol{x},t;\boldsymbol{x'},t') = \langle \boldsymbol{x},t|\boldsymbol{x'},t'\rangle, \qquad (1.7)$$

of a transmission amplitude of a particle or excitation between the points $(\boldsymbol{x'},t')$ and $(\boldsymbol{x},t)$. In order to extract information about the system, we look at two process: On the one hand adding one extra particle to the system, letting it propagate from $(\boldsymbol{x'},t')$ to $(\boldsymbol{x},t)$ and then taking it away and on the other hand extracting one particle—creating a hole—, letting the hole propagate from $(\boldsymbol{x'},t')$ to $(\boldsymbol{x},t)$ and then take it away by inserting a particle. Both processes are described by the *one-particle causal Green's function*,

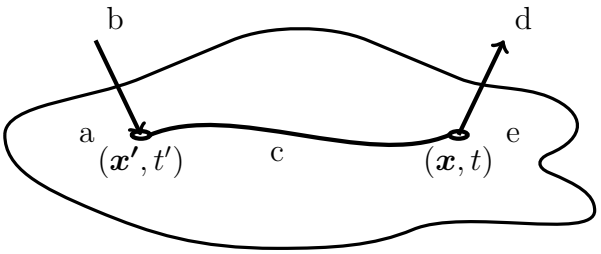

Figure 1.5: Visualization of the one particle Green's function.

$$G(\boldsymbol{x},t;\boldsymbol{x'},t') = -\mathrm{i}\langle\hat{\Psi}_\sigma(\boldsymbol{x},t)\hat{\Psi}^\dagger_{\sigma'}(\boldsymbol{x'},t')\rangle\Theta(t-t') \mp \mathrm{i}\langle\hat{\Psi}^\dagger_{\sigma'}(\boldsymbol{x'},t')\hat{\Psi}_\sigma(\boldsymbol{x},t)\rangle\Theta(t'-t) \quad (1.8)$$

$$\equiv \langle\hat{T}\hat{\Psi}_\sigma(\boldsymbol{x},t)\hat{\Psi}^\dagger_\sigma(\boldsymbol{x'},t')\rangle, \qquad (1.9)$$

where $\hat{\Psi}^\dagger_\sigma(\boldsymbol{x'},t')$ and $\hat{\Psi}_\sigma(\boldsymbol{x},t)$ are the creation and annihilation operators for spin σ at the points $(\boldsymbol{x'},t')$ and $(\boldsymbol{x},t)$, $\Theta(t-t')$ is the Heaviside function and $\hat{T}$ is the time ordering operator. Therefore in Schrödinger's picture for $t'>t$ and a time independent Hamiltonian $\mathcal{H}$ of the system one obtains

$$G(\boldsymbol{x},t;\boldsymbol{x'},t') = -\mathrm{i}\,\langle\underbrace{\mathrm{e}^{\mathrm{i}\mathcal{H}t}}_{\mathrm{e}}\underbrace{\hat{\Psi}_\sigma(\boldsymbol{x})}_{\mathrm{d}}\underbrace{\mathrm{e}^{-\mathrm{i}\mathcal{H}t}\mathrm{e}^{\mathrm{i}\mathcal{H}t'}}_{\mathrm{c}}\underbrace{\hat{\Psi}^\dagger_\sigma(\boldsymbol{x'})}_{\mathrm{b}}\underbrace{\mathrm{e}^{-\mathrm{i}\mathcal{H}t'}}_{\mathrm{a}}\rangle, \qquad (1.10)$$

where the terms **a** - **e** resemble **a:** "$\mathrm{e}^{-\mathrm{i}\mathcal{H}t'}\rangle$"$= |\Psi(t')\rangle$ the initial ensemble state at time t', **b:** adding a particle at $(\boldsymbol{x'},t')$, **c:** $\mathrm{e}^{-\mathrm{i}\mathcal{H}t}\mathrm{e}^{\mathrm{i}\mathcal{H}t'} = \mathrm{e}^{\mathrm{i}\mathcal{H}(t'-t)}$ propagation from time t' to t, **d:** removing a particle at $(\boldsymbol{x},t)$, **e:** the final ensemble state at time t as shown in Fig.**??**. Furthermore $\langle ...\rangle$ is for finite temperature T given by

$$\langle ...\rangle = \frac{1}{\mathrm{Tr}\{\mathrm{e}^{-\beta\mathcal{H}}\}}\mathrm{Tr}\{\mathrm{e}^{-\beta\mathcal{H}}...\} \quad \forall\, T>0, \qquad (1.11)$$

where the *inverse temperature* $\beta = \frac{1}{k_\mathrm{B}T}$ and k_B is Boltzmann's constant. It is often helpful to perform Wick's rotation by the continuation to imaginary time $t=-\mathrm{i}\tau$ and with the convention

$$G(\boldsymbol{x},\tau;\boldsymbol{x}',\tau') = -\mathrm{i}G(\boldsymbol{x},t=-\mathrm{i}\tau;\boldsymbol{x'},t'=-\mathrm{i}\tau'), \qquad (1.12)$$

yields

$$G(\boldsymbol{x},\tau;\boldsymbol{x}',\tau') = -\frac{1}{\mathrm{Tr}\{\mathrm{e}^{-\beta\mathcal{H}}\}}\mathrm{Tr}\{\mathrm{e}^{-\mathcal{H}(\beta-\tau)}\hat{\Psi}_\sigma(\boldsymbol{x})\mathrm{e}^{-\mathcal{H}(\tau'-\tau)}\hat{\Psi}^\dagger_\sigma(\boldsymbol{x'})\mathrm{e}^{-\mathcal{H}\tau)}\}. \qquad (1.13)$$

Due to space and time translation invariance one may perform the transformation $G(\boldsymbol{x}, \tau; \boldsymbol{x'}, \tau') \to G(\boldsymbol{x} - \boldsymbol{x'}, \tau - \tau')$, where the amount of arguments is reduced. [1] The cyclic property for fermions

$$G(\boldsymbol{x}, \tau - \beta) = -G(\boldsymbol{x}, \tau) \tag{1.14}$$

finally leads to the *Green's function in Matsubara frequencies*

$$G(\boldsymbol{x}, \tau) = \frac{1}{\beta} \sum_n G(\boldsymbol{x}, \mathrm{i}\omega_n) \mathrm{e}^{-\mathrm{i}\omega_n \tau}, \tag{1.15}$$

$$G(\boldsymbol{x}, \mathrm{i}\omega_n) = \int_0^\beta \mathrm{d}\tau \, G(\boldsymbol{x}, \tau) \mathrm{e}^{\mathrm{i}\omega_n \tau}, \tag{1.16}$$

where the *fermionic Matsubara frequencies* are given by

$$\omega_n = \frac{\pi}{\beta}(2n + 1). \tag{1.17}$$

These Green's functions represent *dressed propagators*, which account for all the interaction one particle has with the system during propagation. The dressed Green's function G^0 can be put into a relation with the bare Green's function G—propagation without interaction of the particle with the system—and the *self-energy* Σ—representing the effect of the interaction of the particle with the system on the propagation—by the *Dyson equation*.

$$G = G^0 + G^0 \Sigma G \tag{1.18}$$

The dressed propagator can be diagrammatically written as an infinite sum of all possible interactions: As a final remark one arrives from the Heisenberg equation of motion for independent particles,

$$[\frac{\mathrm{d}}{\mathrm{d}\tau} + \mathcal{H}(\boldsymbol{x})] G^0(\boldsymbol{x}, \tau) = -\delta(\tau)\delta(\boldsymbol{x}), \tag{1.19}$$

through Fourier transformation at an expression for the *bare Green's function*,

$$G^0(\boldsymbol{k}, \mathrm{i}\omega_n) = \frac{1}{\mathrm{i}\omega_n - \epsilon_k + \mu}. \tag{1.20}$$

With the argument that there exists a one-to-one relation between energy levels of the interacting and the non-interacting system one finds a similar expression for the *interacting lattice Green's function*

$$G(\boldsymbol{k}, \mathrm{i}\omega_n) = \frac{1}{\mathrm{i}\omega_n - \epsilon_k + \mu - \Sigma(\mathrm{i}\omega_n)}, \tag{1.21}$$

which is consistent with Dyson's equation. (**?**)

[1] We shall change notation slightly, so that τ now denotes the difference in imaginary time previously denoted by $\tau - \tau'$ and similarly $\boldsymbol{x} - \boldsymbol{x'} \to \boldsymbol{x}$.

1.1.4 Self-consistency loop

The introduced formalism is used to describe the dynamics of a system described by the Hubbard Hamiltonian in Eq. (**??**). In practice, mapping the Hubbard model onto an AIM means to determine the mean field bare Green's function self-consistently by iterating the loop shown in Fig. **??**. The loop is entered through guessing an initial Green's function $G^{\mathrm{loc}}_{(\mathrm{i}\omega_n)}$ e.g. by setting the *self-energy* $\Sigma(\mathrm{i}\omega_n) = 0$. The bare Green's function is passed on to the *impurity solver*, which can be realized by a *Quantum Monte Carlo* method (CT-QMC), *iterative perturbation theory* (IPT) and in certain cases by analytic calculations, as well as other methods. (**?**) For a deeper understanding A. Georges *et al.* (**?**) provides an excellent introduction to DMFT of strongly correlated fermion systems and the limit of infinite dimensions.

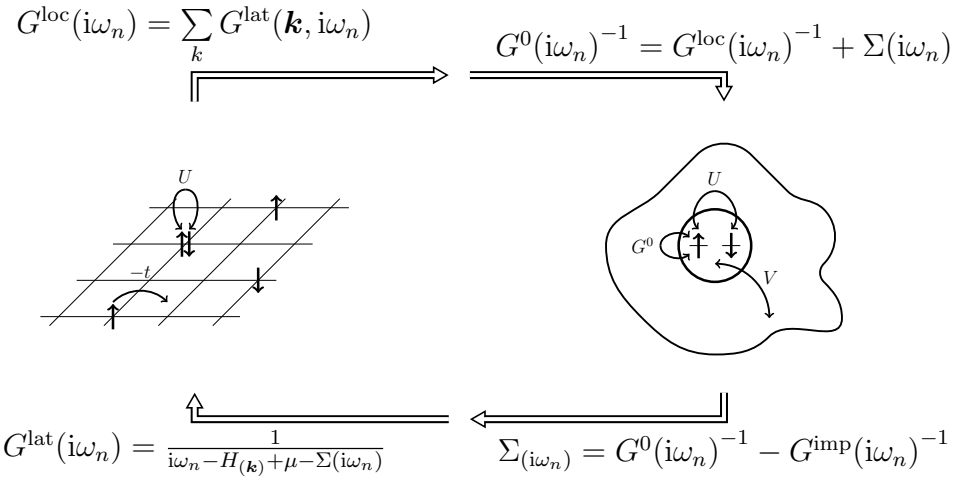

Figure 1.6: Self-consistency loop

1.1.5 Falicov-Kimball model

One of the lattice models which has an analytic solution of the impurity model is represented by the *Falicov-Kimball* (FK) *model*. It can be seen as an "amputated" Hubbard model, since it is obtained by freezing the spin up electrons of the Hubbard model. This is displayed by the Hamiltonian

$$\mathcal{H}_{\mathrm{FK}} = -t \sum_{<i,j>} \left[\hat{c}_i^\dagger \hat{c}_j + \hat{c}_j^\dagger \hat{c}_i\right] + U \sum_i \left(\hat{c}_i^\dagger \hat{c}_i \hat{f}_i^\dagger \hat{f}_i\right) + \epsilon_f \sum_i \left(\hat{f}_i^\dagger \hat{f}_i\right) - \mu \sum_i \left(\hat{c}_i^\dagger \hat{c}_i + \hat{f}_i^\dagger \hat{f}_i\right), \tag{1.22}$$

where $\hat{c}_i^\dagger$ and $\hat{c}_i$ are the creation and annihilation field operators of the conducting spin down electrons and $\hat{f}_i^\dagger$ and $\hat{f}_i$ are the creation and annihilation field operators of the frozen or fixed spin up electrons on the lattice site i. ϵ_f is the on-site energy of the fixed electrons, while an on-site energy of the conducting electrons is absorbed by the chemical potential μ. Mapping the FK model onto an AIM is done by substituting the

Hamiltonian in Eq. (**??**) by a *resonant level model* (RLM), yielding

$$\mathcal{H}_{\mathrm{FK}}^{\mathrm{imp}} = \sum_l \left[(\epsilon_l - \mu)\, \hat{c}_l^\dagger \hat{c}_l - t_l\, \hat{c}_l^\dagger \hat{c} - t_l^*\, \hat{c}^\dagger \hat{c}_l \right] + U \left(\hat{c}^\dagger \hat{c} \hat{f}^\dagger \hat{f} \right) + \epsilon_f \left(\hat{f}^\dagger \hat{f} \right) - \mu \left(\hat{c}^\dagger \hat{c} + \hat{f}^\dagger \hat{f} \right), \tag{1.23}$$

where l labels the bath-states, ϵ_l is the corresponding bath-energy level and t_l (and t_l^* respectively) is the hybridization between the impurity site and the bath-state l. The first term mimics the rest of the lattice. It corresponds to the interaction of the electron on the impurity site with the external bath, while the second term is the Coulomb term, the third term corresponds to the on-site energy of a fixed electron, and the last term corresponds to the chemical potential μ acting only on the impurity site. The RLM impurity site Green's function $G_{\mathrm{RLM}}^{\mathrm{imp}}(\tau)$ in imaginary time τ is defined as

$$G_{\mathrm{RLM}}^{\mathrm{imp}}(\tau) \equiv \langle \hat{c}(\tau) \hat{c}^\dagger(0) \Theta(\tau) - \hat{c}^\dagger(0) \hat{c}(\tau) \Theta(-\tau) \rangle. \tag{1.24}$$

After some calculations one arrives at the RLM impurity site Green's function in Matsubara frequencies,

$$\mathrm{i}\omega_n G_{\mathrm{RLM}}^{\mathrm{imp}}(\mathrm{i}\omega_n) = \sum_l \frac{t_l^* t_l}{\mathrm{i}\omega_n - \epsilon_l + \mu}\; G_{\mathrm{RLM}}^{\mathrm{imp}}(\mathrm{i}\omega_n) + U(0 \vee 1)\; G_{\mathrm{RLM}}^{\mathrm{imp}}(\mathrm{i}\omega_n) - \mu\; G_{\mathrm{RLM}}^{\mathrm{imp}}(\mathrm{i}\omega_n) + 1, \tag{1.25}$$

where $U(0 \vee 1)$ denotes that U is present in the case of a fixed electron occupying the impurity site and zero otherwise. Eq. (**??**) allows the definition of the *hybridization function* $\Delta(\mathrm{i}\omega_n)$,

$$\Delta(\mathrm{i}\omega_n) \equiv \sum_l \frac{t_l^* t_l}{\mathrm{i}\omega_n - \epsilon_l + \mu}, \tag{1.26}$$

yielding

$$G_{\mathrm{RLM}}^{\mathrm{imp}}(\mathrm{i}\omega_n) = \frac{1}{\mathrm{i}\omega_n - \Delta(\mathrm{i}\omega_n) - U(0 \vee 1) + \mu}. \tag{1.27}$$

If p is the *average occupation* of the impurity site by a fixed electron and the bare Green's function in Matsubara frequencies is defined as

$$G^0(\mathrm{i}\omega_n) = \frac{1}{\mathrm{i}\omega_n - \Delta(\mathrm{i}\omega_n) + \mu} \tag{1.28}$$

the *impurity Green's function* is given by

$$G^{\mathrm{imp}}(\mathrm{i}\omega_n) = \frac{p}{G^0(\mathrm{i}\omega_n)^{-1}} + \frac{(1-p)}{G^0(\mathrm{i}\omega_n)^{-1} - U}. \tag{1.29}$$

The calculations are carefully carried out and presented in more detail in the diploma thesis by T. Ribic in Ref. (**?**). For more insight on the exact DMFT of the FK model please refer to the comprehensive paper by J. K. Freericks and V. Zlatić in Ref. (**?**).

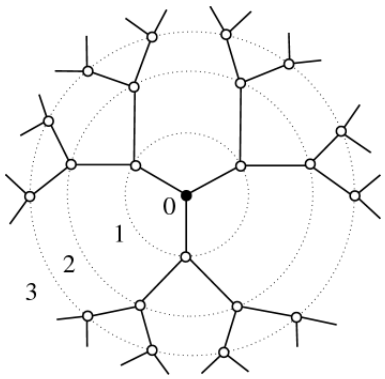

Figure 1.7: Bethe lattice (**?**)

1.2 Bethe lattice

The system's underlying properties are given by its lattice and its symmetries. In Fig. **??** we see a square lattice, which is a special case of the general d dimensional *hypercubic* (hc) lattice. The d dimensional hc lattice is spanned by d orthonormal primitive lattice vectors. The shortest lattice vector defines NNs which we need to describe NN hopping with amplitude $-t$. In general one may define next-nearest-neightbor hopping and so forth, however their amplitude of hopping is assumed to decrease with increasing distance. Mapping a lattice model onto a AIM requires to find the corresponding *density of states* (DOS) to the lattice type and dimension. As discussed in **??** DMFT is exact for $d \to \infty$ and thus the DOS for $d \to \infty$ is of interest. However the DOS of the hc lattice has unpleasant properties. It is Gaussian shaped and thus has an in principle infinite bandwidth. These tails of the hc DOS motivate the introduction of a some what unphysical pseudo lattice: The Bethe lattice.[2]

The Bethe lattice is a special case of the Cayley Tree where each site is surrounded by Z NNs and where no closed loops are formed. In $d = 1$, i.e. $Z = 2$, this corresponds to a usual, chain-like lattice. However in $Z > 2$ it is not a regular lattice as shown in Fig. **??** for $Z = 3$. For $d \to \infty$, i.e. $Z \to \infty$, the Bethe DOS is given by

$$D(\varepsilon) = \frac{2}{\pi D}\sqrt{1 - \left(\frac{\varepsilon}{D}\right)^2}, \tag{1.30}$$

where ε is the energy and D is the *half-bandwidth*—marking the sharp edges of this semi-elliptic DOS shown in Fig. **??** on the right. The half bandwidth D of the Bethe DOS is connected to the hopping amplitude $-t$ of the Hubbard model by the relation $D = 2t$. And respectively the half-bandwidth is directly proportional to the kinetic energy of the system, $E_{\text{kin}} \propto D$. In order to compare results of different DOS in a meaningful way one defines the effective bandwidth

$$W = 4\sqrt{\int_{-\infty}^{\infty} \mathrm{d}\varepsilon\, \varepsilon^2 D(\varepsilon)}, \tag{1.31}$$

[2]Suggested in 1935 by H. A. Bethe. (**?**)

which is for the Bethe DOS given by $W = 2D$. The half-bandwidth is related to the hopping term of the Hamiltonian as $D = 2|t|$. The symmetry of the Bethe lattice causes the system to be separable into sub-lattices of opposite local magnetic moment—corresponding to anti-ferromagnetic behavior—for temperatures below the critical Néel temperature, $T < T_N$. Interestingly the same semi-elliptic DOS is expected for an arbitrary topology—e.g. a fully connected lattice—as long as there is randomness of the hopping $-t_{ij}$, where i, j are NNs and the mean vanishes, $\langle t_{ij} \rangle = 0$. For these lattices one can generally not expect Néel order for any finite temperature.

One finds an analytic expression for the *local Green's function* by rewriting the sum over all momenta $\boldsymbol{k}$ of the lattice Green's function

$$G^{\mathrm{loc}}(\mathrm{i}\omega_n) = \sum_k G^{\mathrm{lat}}_{(\boldsymbol{k},\mathrm{i}\omega_n)} = \sum_k \left(\zeta_n - \varepsilon_k\right)^{-1} \tag{1.32}$$

$$\approx \int_{-D}^{D} \mathrm{d}\varepsilon \frac{N(\varepsilon)}{\zeta_n - \varepsilon} = \frac{2\zeta_n}{D^2}\left(1 - \sqrt{1 - \frac{D^2}{\zeta_n^2}}\right), \tag{1.33}$$

where $\zeta_n = \mathrm{i}\omega_n + \mu - \Sigma(\mathrm{i}\omega_n)$ was defined for convenience. For more details on how to arrive at the Bethe DOS and applications—e.g. mapping it onto a hc lattice and thus define transport properties—refer to chapter 2 of the Ph.D thesis by N. Blümer in Ref. (**?**). Furthermore to exploit on the link to the Mott transition discussed in the next chapter refer to the paper by A. Georges *et al.* in Ref. (**?**).

1.3 Mott transition

Before one continues with reading it is important to be familiar with basic Fermi Liquid Theory. Thereby key words such as the quasiparticle concept, excitation-hole pair creation and the Kondo effect may be exploited.

With this fundament we shall discuss a qualitative picture of the Mott phase transition in the Hubbard model. Suppose at time $t = -\infty$ there was no particle-particle interaction and the system—described by $\mathcal{H}_0$—can be solved exactly. Now the interaction is switched on adiabatically—described by $\mathcal{H} = \mathcal{H}_0 + \lambda(t)\mathcal{V}$—, so that no energy level cross.[3] There exists a one-to-one relation between energy level before and after the adiabatic switch on. This argument has already been used in **??** and is referred to as *adiabatic concept*. Because states of different symmetry can not mix due to selection rules, it is possible that their energy level cross without loosing the one-to-one relation. If energy level cross at a critical interaction strength λ_{c} the system changes its ground state to a different symmetry. This process is called *spontaneous symmetry breaking* and describes a phase transition.

In the Hubbard model on the Bethe lattice introduced in Section **??** 4 different phases can be distinguished: A high-temperature paramagnetic metallic phase, a high-temperature paramagnetic insulating phase, a low-temperature anti-ferromagnetic insulating phase and magnetically frustrated anti-ferromagnetic metallic phase. However in the scope of this work we shall ignore—or rather suppress—Néel order in order to find

[3] $\lambda(t) = \mathrm{e}^{-\theta|t|}$, where θ can be arbitrarily small and $0 \leqslant \lambda \leqslant 1$.

the Mott transition from a paramagnetic metallic phase to a paramagnetic insulating phase at low temperatures. This may seem unphysical at first, however as motivated in Section **??** this merely suggests a system on a fully connected lattice with semi-elliptic DOS.

In Fig. 30 of Ref. **?** a qualitative picture of the Mott transition from a metal to an insulator at $T = 0$ is shown. The transition proceeds as follows: For the limit of no interaction, i.e. $U = 0$, the DOS is unchanged a semi-elliptic shape, which is at half-filling centred at the chemical potential and hence metallic behavior. As the interaction is turned on the *upper* and the *lower Hubbard bands* wander off each centered at $\pm\frac{U}{2}$ leaving behind only the *quasiparticle peak* at the Fermi surface as a display of the Kondo effect. The height of the quasiparticle peak remains unchanged—this is called *pinning*—while the width is determined by the Kondo temperature of the impurity, which is related to the *quasiparticle residue* Z or Z*-factor*. The Z-factor is given by the low frequency behavior of the self-energy of a local Fermi liquid:[4]

$$\Re\left\{\Sigma(\omega + \mathrm{i}0+)\right\} = \frac{U}{2} + (1 - \frac{1}{Z})\omega + \mathcal{O}(\omega^3). \tag{1.34}$$

It allows to make statements about the renormalization of the system, since it is related to the *effective mass* m^* of the quasiparticle by

$$\frac{1}{Z} = \frac{m^*}{m} \tag{1.35}$$

and to the *renormalized Fermi energy* by

$$\varepsilon_{\mathrm{F}}^* = ZD, \tag{1.36}$$

which also defines the Kondo temperature. As the interaction U increases the quasiparticle peak gets narrower, i.e. the quasiparticles get heavier, and finally vanish at a *critical interaction strength* U_{c2}. As there is no weight at the Fermi surface the system entered the insulating phase. The gap between the Hubbard bands is of the order of $U - 2D$. By further increasing U the hopping becomes negligible and we approach the atomic limit discussed in **??**.

Going back from the insulating phase to the metallic phase implies decreasing U. Coming now from the atomic limit no quasiparticle peak appears until the Hubbard bands meet at the chemical potential and the metallic phase is entered. It happens at the *critical interaction strength* U_{c1}. Generally the critical interaction strength U_{c1} is not equal to U_{c2}, $U_{\mathrm{c1}} \neq U_{\mathrm{c2}}$. Clearly it is a first order phase transition with a jump in the *double occupancy* of the impurity as the quasiparticle peak abruptly vanishes. The *coexistence region* refers to the values $U_{\mathrm{c1}} \leq U \leq U_{\mathrm{c2}}$, where the system has a metallic as well as an insulating solution.

For finite temperatures one finds a phase diagram in which for $T < T_{\mathrm{c}}$ exists a first order phase transition with coexistence region and for $T > T_{\mathrm{c}}$ exists a not sharply

[4]The statement is about the self-energy in real frequencies.

outlined *cross over region*. The cross over from the metallic to the insulating phase proceeds by a continuous decrease of the double occupancy.

In order to find more explanations on the adiabatic concept, phase transitions, the Landau Fermi liquid theory or local moments as well as the Kondo effect the soon to be published Introduction to Many Body Physics by P. Coleman in Ref. **?** is recommended. Furthermore the connection to the Mott transition of the Hubbard model with a Bethe DOS is again nicely described in the paper by A. Georges *et al.* in Ref. (**?**).

2 Computer programs

This chapter describes two programs, which can solve a self consistent loop as displayed in Fig. **??**. Firstly bethe-phasediagram-14-04-15.py which can solve the mapping of the lattice model onto the impurity model in FK model. And secondly the pre-existing w2dynamics, which has been slightly modified in order to investigate the behavior of the Mott transition of the Hubbard model towards the FK model.

2.1 Falicov-Kimball

In order to look at the Mott-like transition of the FK model one can follow the self-consistent loop in Fig. **??**. The loop is entered by setting up all fermionic Matsubara frequencies using Eq. (**??**), starting from a non-interacting solution by setting the self-energy in Matsubara frequencies (siw) equal zero and using the analytic result for the local Green's function in Matsubara frequencies on the Bethe lattice found in Eq. (**??**) by approximating the sum over all momenta (first_gloc by the function Green_local_analytically). This gives rise to the first hybridization function given by rearranging Eq. (**??**) (fiw by the function hybridization). In this step the Dyson Eq. has been used implicitly. As the self-energy is zero the local Green's function is exactly equal to the bare Green's function. Within the loop the impurity solver is represented by the function Green_local using Eq. (**??**) (glocold), which is unique to the FK model. At the same time the bare Green's function is computed (giw). The local and the bare Green's function are now used to calculate the self-energy (siw) by using the Dyson Eq. and subsequently using the self-energy to compute a new local Green's function in Matsubara frequencies (gloc) by applying once again the analytically solved integral in Eq. (**??**). From this point one finds a new hybridization (fiw) and can repeat the loop until self-consistency is reached, but also the local Green's function in imaginary time (gtau) can be computed by performing a Fourier transformation. However a little trick is used: To take care of the asymptotic behavior $\frac{1}{\mathrm{i}\omega_n}$ it is first subtracted and then added afterwards,

$$G(\tau) = \mathcal{F}\left(G^{\mathrm{imp}}(\mathrm{i}\omega_n)^{-1} - \frac{1}{\mathrm{i}\omega_n}\right) - \frac{1}{2}. \tag{2.1}$$

This loop is the basis of the Python script bethe-phasediagram-14-04-15.py, which can be found in Appendix **??**. In the first two sections—separated by ###...#—the half-bandwidth D, inverse temperature β, the number of iteration steps (DMFTsteps), some file name prefix for the output, the number of discrete Matsubara frequencies and imaginary time coordinates (Niw and Ntau), the values of interaction strength (U) and the average occupation probability (p) are set. In the third section libraries are imported and functions are defined to subsequently perform the described loop for all U values.

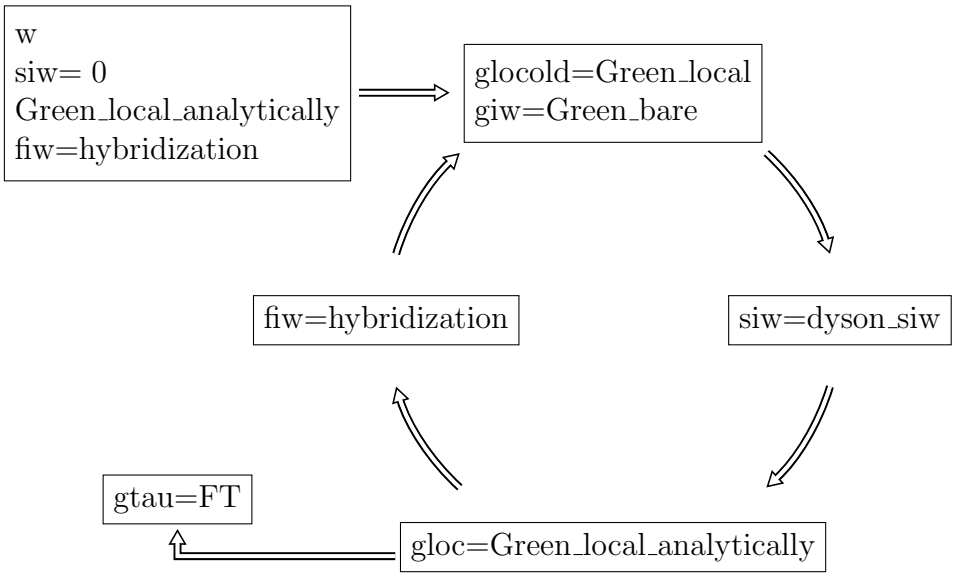

Figure 2.1: The self consistent loop used in bethe-phasediagram-14-04-15.py to investigate the Mott-like transition of FK model. A summary of the used functions is presented in Table **??**.

w	$\omega_n = \frac{\pi}{\beta}(2n+1)$
Green_local_analytically	$G^{\mathrm{loc}}(\mathrm{i}\omega_n) = \frac{2\zeta_n}{D^2}\left(1-\sqrt{1-\frac{D^2}{\zeta_n^2}}\right)$, where $\zeta_n = \mathrm{i}\omega_n + \mu - \Sigma(\mathrm{i}\omega_n)$
gfw2g0w	$G^0(\mathrm{i}\omega_n)^{-1} = G^{\mathrm{loc}}(\mathrm{i}\omega_n)^{-1} + \Sigma(\mathrm{i}\omega_n)$
fiw=hybridization	$\Delta(\mathrm{i}\omega_n) = \mathrm{i}\omega_n + \mu - G^0(\mathrm{i}\omega_n)^{-1}$
glocold = Green_local	$G^{\mathrm{imp}}(\mathrm{i}\omega) = \frac{p}{G^0(\mathrm{i}\omega_n)^{-1}} + \frac{(1-p)}{G^0(\mathrm{i}\omega_n)^{-1}-U}$
giw=Green_bare	$G^0(\mathrm{i}\omega_n) = \frac{1}{\mathrm{i}\omega_n - \Delta(\mathrm{i}\omega_n)+\mu}$
gtau=FT	$G(\tau) = \mathcal{F}\left(G^{\mathrm{imp}}(\mathrm{i}\omega_n)^{-1} - \frac{1}{\mathrm{i}\omega_n}\right) - \frac{1}{2}$
dyson_siw	$\Sigma(\mathrm{i}\omega_n) = G^0(\mathrm{i}\omega_n)^{-1} - G^{\mathrm{imp}}(\mathrm{i}\omega)^{-1}$

Table 2.1: A summary of the functions used to perform the self consistent loop of bethe-phasediagram-14-04-15.py displayed in Fig. **??**.

And furthermore the local Green's function of the impurity, the self-energy, local Green's function of the lattice and the hybridization in Matsubara frequencies, as well as the local Green's function in imaginary time are stored. In the final section a small overview is send to the terminal, the local Green's function in imaginary time and the self energy in Matsubara frequencies are stored in txt files labelled by the according U value and all stored functions may be plotted. The same loop has been used and published by Ling Chen, B. A. Jones and J. K. Freericks—Ref. **?**.

2.2 w2dynamics

The w2dynamics program performs a self consistent loop as shown in Fig. **??** for the Hubbard model. The impurity solver is realized by a continuous time quantum Monte Carlo (CT-QMC) method and one of its classes—BetheLattice—enables calculations on the Bethe lattice for arbitrary half-bandwidth. In the scope of this work some adjustments have been made: The class FKBetheLattice was added. Its code can be found in Appendix **??**. The class is an extension to the class BetheLattice and allows to choose different half-bandwidths for each spin and hence to simulate the limit between the Hubbard model—with two equally mobile spins—and the FK model—with one frozen spin.[1]

The following steps implement the new class in an older version of the code:

- \w2dynamics\auxiliaries\configspec :
  old:
  ```
  DOS =
  option('flat','semicirc','ReadIn','ReadInSO','Bethe','Bethe_in_tau',
  'EDcheck','nano','CoulvsKan','readDelta' ,default='Bethe')
  ```
  new:
  ```
  DOS =
  option('flat','semicirc','ReadIn','ReadInSO','Bethe','FKBethe',
  'Bethe_in_tau','EDcheck','nano','CoulvsKan','readDelta' ,default='Bethe')
  ```

- \w2dynamics\auxiliaries\lattices.py :
  Insert the class FKBetheLattice in Appendix **??**.
  And add
  `'FKBethe': FKBetheLattice`
  to `str2lat` at the end.

- Do not forget performing `./install.sh`

As a final remark an important step shall be pointed out: On the Bethe lattice the Mott transition as shadowed by an antiferromagnetic dome. In order to suppress this behavior the hybridization in imaginary time (ftau) is symmetrised at $\frac{\beta}{2}$. This forces the local Green's function in imaginary time to stay symmetric around $\frac{\beta}{2}$ and thus both spins stay degenerate. For a better understanding of these physical arguments refer to Section **??**.

[1] Winter is coming.

3 Results

In this chapter the observables, i.e. the quantities connected to the self-energy in Matsubara frequencies and to the local Green's function in imaginary time as well as the occupancy, shall be introduced in a qualitative manner. It will enable us to subsequently interpret the results produced by the programs described in chapter **??**.

3.1 Properties of observables

3.1.1 Self energy in Matsubara frequencies

The self-energy is used as an indicator of local Fermi liquid behavior. On the Matsubara frequency-axis the low-frequency behavior of the imaginary part of the self-energy is given by

$$\Im\Sigma(\mathrm{i}\omega_n) = -\mathrm{i}\gamma - \mathrm{i}\alpha\omega_n + \mathcal{O}(\omega_n^2), \tag{3.1}$$

where the off set γ is due to the imaginary part of the self-energy on the real frequency axis, which is related to the *life-time of a quasi particle*. The linear contribution α results from the real part of the self-energy on the real frequency axis and has a simple relation to the quasi particle residue as one finds by comparison to Eq. (**??**),

$$Z = (1+\alpha)^{-1}. \tag{3.2}$$

The values are extracted from data by the code in Appendix **??** which uses a linear fitting to the first two values $\Im\Sigma(\mathrm{i}\omega_1)$ and $\Im\Sigma(\mathrm{i}\omega_2)$.

Fig. **??** (a) shows a typical example of local Fermi liquid like behavior of a renormalized system in the paramagnetic, metallic phase. If the Fermi liquid breaks down due to a phase transition into the paramagnetic insulating phase, the self-energy diverges for low frequencies—forming a pole for $|\omega| \to 0$ as shown in Fig. **??** (b).[1] In both cases the asymptotic behavior for $\mathrm{i}\omega_n \to \infty$ is given by $A + \frac{B}{\mathrm{i}\omega_n}$, which is consistent with the properties of the Green's function in Matsubara frequencies and is dictated by the value of interaction strength, i.e. by $\frac{U^2 n(n-1)}{\mathrm{i}\omega_n} = \frac{U^2}{4\,\mathrm{i}\omega_n}$ at half-filling.

Fig. **??** shows the quasi particle residue Z as a function of the interaction strength U at different temperatures, $\beta = 100$ and $\beta = 20$. If the value of Z is approaches 0, the imaginary part of the self-energy diverges at low Matsubara frequencies. The divergence corresponds to the break down of the Fermi Liquid behavior—i.e. the quasi particle concept—and hence the definition of the quasi particle residue in Eq. (**??**). Even though

[1] Strictly speaking there can only be divergence of the self-energy on the real frequency axis for $|\omega| \to 0$ since there is no fermionic Matsubara frequency at zero, $|\mathrm{i}\omega_n| \neq 0$. However one can see the asymptotics towards this behavior.

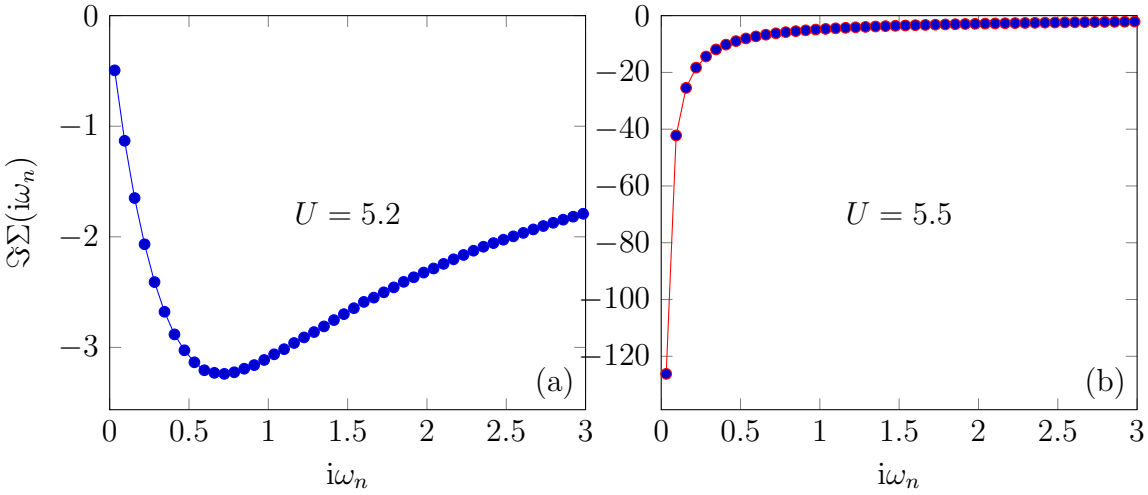

Figure 3.1: The imaginary part of the self-energy in Matsubara frequencies of the Hubbard model at inverse temperature $\beta = 100$, with half-bandwidth $D = 2$ on the Bethe lattice with interaction strength (a) $U = 5.2$ corresponding to a paramagnetic, metallic phase, and (b) $U = 5.5$ corresponding to a paramagnetic, insulating phase.

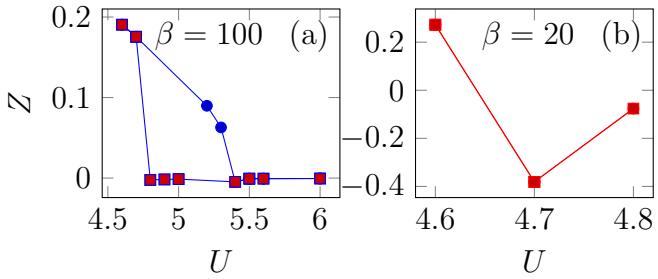

Figure 3.2: The Z-factor extracted from the imaginary part of the self-energy in Matsubara frequencies of the Hubbard model with half-bandwidth $D = 2$ on the Bethe lattice as a function of the interaction strength U at the inverse temperature (a) $\beta = 100$ corresponding to a Mott transition with coexistence region for $4.75 \pm 0.05 < U < 5.35 \pm 0.05$, and (b) $\beta = 20$ corresponding to a cross over.

the definition breaks down the data point is included in the plot illustrative reasons. Negative values of Z—as it is the case for $\beta = 20$ and $U = 4.7$ in Fig. **??** (b)—often appear in a system in which the Fermi liquid theory is of limited validity. The reason for the negative value is that at high temperatures the spacing of the Matsubara frequency is too large to capture the linear low-frequency behavior that correspond to Fermi liquid properties. The quasi particle concept holds, however the excitation do not have infinite life-time and thus there is no pinning of the quasi particle peak. Far above the critical temperature T_c the damping of the quasi particle peak can suppress it entirely. It leads to a very similar spectral function as one finds in the FK model featuring no quasi particle peak but the Hubbard bands. [2] Lastly, any positive finite value describes the renormalization of the system.

[2]The state of art is that in the Hubbard model at high temperatures quasiparitcles exist with infinitely short life-time, as compared to the FK model where quasiparticle excitations are believed to be suppressed. It corresponds to the mickey mouse picture that the Kondo effect cannot take place if one spin is frozen and thus no Kondo-peak or equivalently quasiparticle peak occures. As we will see later, the interpretation of the FK model cannot hold.

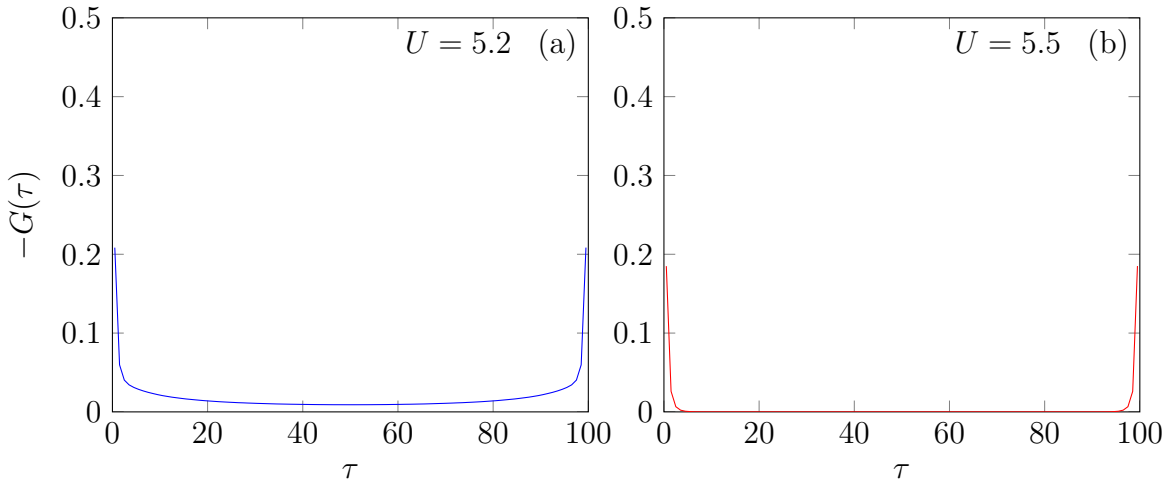

Figure 3.3: The local Green's function in imaginary time of the Hubbard model at inverse temperature $\beta = 100$, with half-bandwidth $D = 2$ on the Bethe lattice computed with 100 τ ticks with interaction strength (a) $U = 5.2$ corresponding to a paramagnetic, metallic phase, and (b) $U = 5.5$ corresponding to a paramagnetic, insulating phase.

3.1.2 Local Green's function in imaginary time

The local Green's function in imaginary time is the default measurement in w2dynamics within the impurity solver. It is used to perform the analytic continuation and find the spectral function as described in **??**, but can already be valued for physical interpretation: The values $G(\tau = 0)$ and $G(\tau = \beta)$ must add up to the absolute value of 1, $|G(\tau = 0) + G(\tau = \beta)| = 1$, and indicate the filling of the system. At half-filling this translates to the condition

$$G(\tau = 0) = G(\tau = \beta) = 0.5. \tag{3.3}$$

However in numerical methods it is often cut off due to binning as it is also the case in Fig. **??**. The value $G(\tau = \beta/2)$ is an indicator for the spectral weight in a small interval, $k_\mathrm{B}T$, around the Fermi surface as one sees by comparison of the paramagnetic metallic solution in Fig. **??** (a) to the paramagnetic insulating solution in Fig. **??** (b).[3] More physical properties can be found by plotting on a logarithmic scale as shown in Fig. **??**. The partly linear behavior on this scale is a result of the main energy level contributions. For more details of the interpretation one has to consider the Källén-Lehmann representation, but is best advised to refer to the Ph.D thesis by M. Wallerberger in Ref. **?**.

[3]The sign of the function is merely convention and should not be taken too seriously.

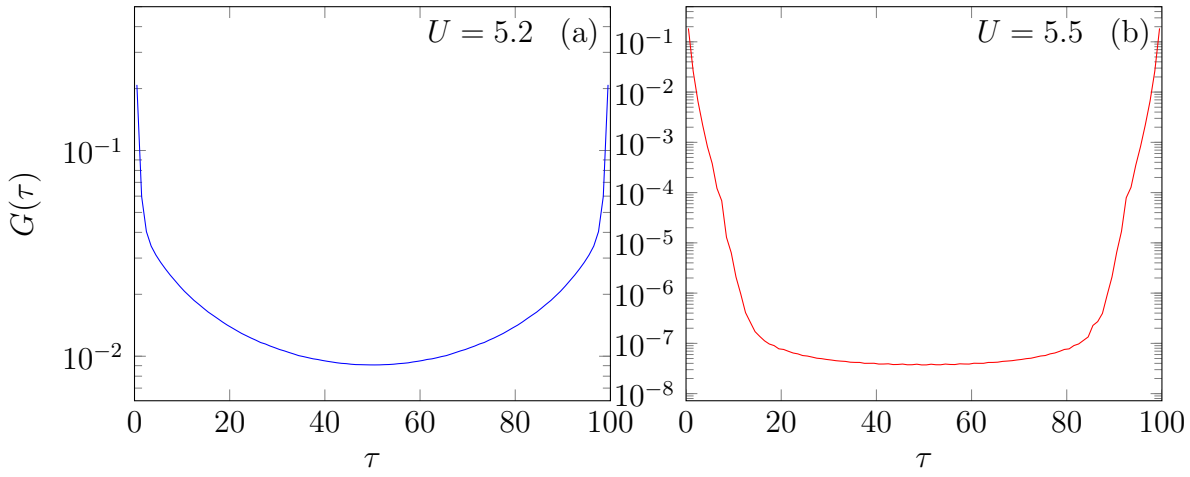

Figure 3.4: The local Green's function in imaginary time of the Hubbard model at inverse temperature $\beta = 100$, with half-bandwidth $D = 2$ on the Bethe lattice with interaction strength (a) $U = 5.2$ corresponding to a paramagnetic, metallic phase, and (b) $U = 5.5$ corresponding to a paramagnetic, insulating phase on a logarithmic scale.

3.1.3 Occupancy

The occupancy is a real and symmetric matrix of the form $\langle n_\sigma n_{\sigma'} \rangle$, where the off-diagonal elements are called double occupancy, i.e. $\langle n_\uparrow n_\downarrow \rangle = \langle n_\downarrow n_\uparrow \rangle$. In Fig. **??** the double occupancy is shown as a function of the interaction strength going from the metallic phase to the insulating phase and vis versa for two different temperatures, $\beta = 100$ and $\beta = 20$. As $\beta = 100$ the Hubbard model undergoes a Mott transition. It causes the formation of a hysteresis due to the coexistence region as shown in Fig. **??** (a). For $\beta = 20$ the system passes the cross over region, where the double occupancy is a continuous function of the interaction strength as shown[4] in Fig. **??** (b).

3.1.4 Spectral function

In order to obtain the spectral function $A(\omega)$ from imaginary time—or equivalently of Matsubara frequencies—one needs to do an analytic continuation to real frequencies. More precisely in the case of an analytic continuation of the local Green's function in imaginary time the spectral function needs to be extracted from the integral

$$G(\tau) = \int \mathrm{d}\omega \, \frac{\mathrm{e}^{-\tau\omega}}{1 + \mathrm{e}^{-\beta\omega}} A(\omega), \tag{3.4}$$

which is an under-determined problem if $G(\tau)$ is known on a finite support only. The problem is tackled by the *maximum entropy* (MaxEnt) method.[5] Since it is a stochastic

[4] or rather foreshadowed
[5] Missing ref to first Max ent paper

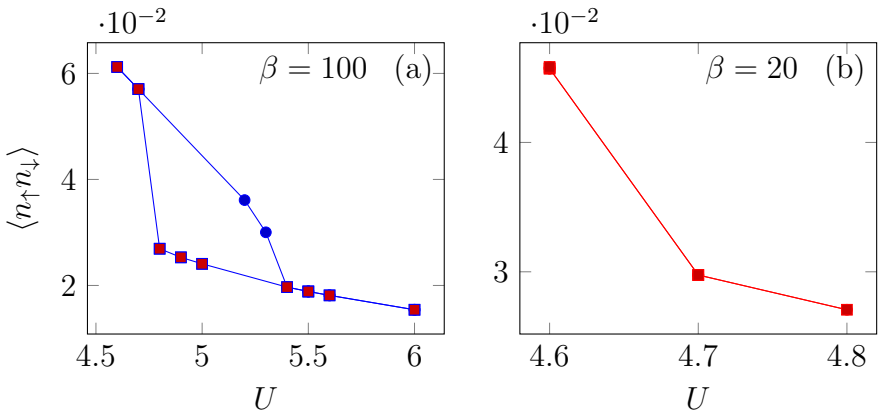

Figure 3.5: The double occupancy $\langle n_\uparrow n_\downarrow \rangle$ as a function of the interaction strength U with half-bandwidth $D = 2$ on the Bethe lattice in the Hubbard model at (a) $\beta = 100$ displaying a hysteresis within the coexistence region, and (b) $\beta = 20$ displaying a continuous cross over.

procedure there is no assurance that the computed spectral function is indeed the best solution. The package used in the scope of this work has been implemented and described in detail by B. Hartl in Ref. **?**.

After this warning the importance of some physical aspects of the spectra shall be stressed. Here, for a discussion of the spectral function near the Mott transition in the Hubbard model shall be pointed to Ref. **?** (Chap. VII. and in particular to Fig. 30 as well as to Chap. **??**).

3.2 Falicov-Kimball

Fig. **??** shows results computed by the code described in Section **??**. The half-bandwidth is set equal to 2, $D = 2$. The local Green's function in imaginary time clearly shows half-filling and gives reason to belief that the system changes its phase from metallic to insulating at $U = 2$, while the range of τ indicates $\beta = 50$. Indeed the imaginary part of the self-energy divergence for values $U > 2$ and the system is therefore insulating. However for values $U < 2$ the self-energy does not show Fermi liquid behavior either, because the slope at low frequencies is positive, i.e. α—as defined in Eq. (**??**)—has the wrong sign. This behavior can be referred to as dirty Fermi liquid, although one should stress that the quasi particle concept is not valid for the FK model. [6] The absence of quasi particles—and hence of the quasi particle peak—causes the phase transition to take place when the Hubbard bands separate. The separation occurs temperature independent and furthermore in the case of half-filling exactly at $U = D$ as shown in Fig. **??** .[7]

The spectral function $A(\omega)$ may be obtained by applying the Box-Muller transformation to the local Green's function in imaginary time in order to get a Gaussian error distribution and subsequently performing MaxEnt. However here shall be pointed to FIG. 12 in Rev. **?**, where J. K. Freericks, V. Zlatić are presenting the spectra for different values of U ranging from 0.5 to 3.0 in steps of 0.5. The same units are chosen so that in Rev. **?** and in this work the transition occurs at $U = 2$.

[6] This is true for all fillings, except $p = 0$ or 1. p is defined in Eq. (**??**).

[7] The T independence can be shown more explicit by a mapping presented in Ref. **?**. However one should keep in mind that the temperature naturally still influences the spacing of Matsubara frequencies.

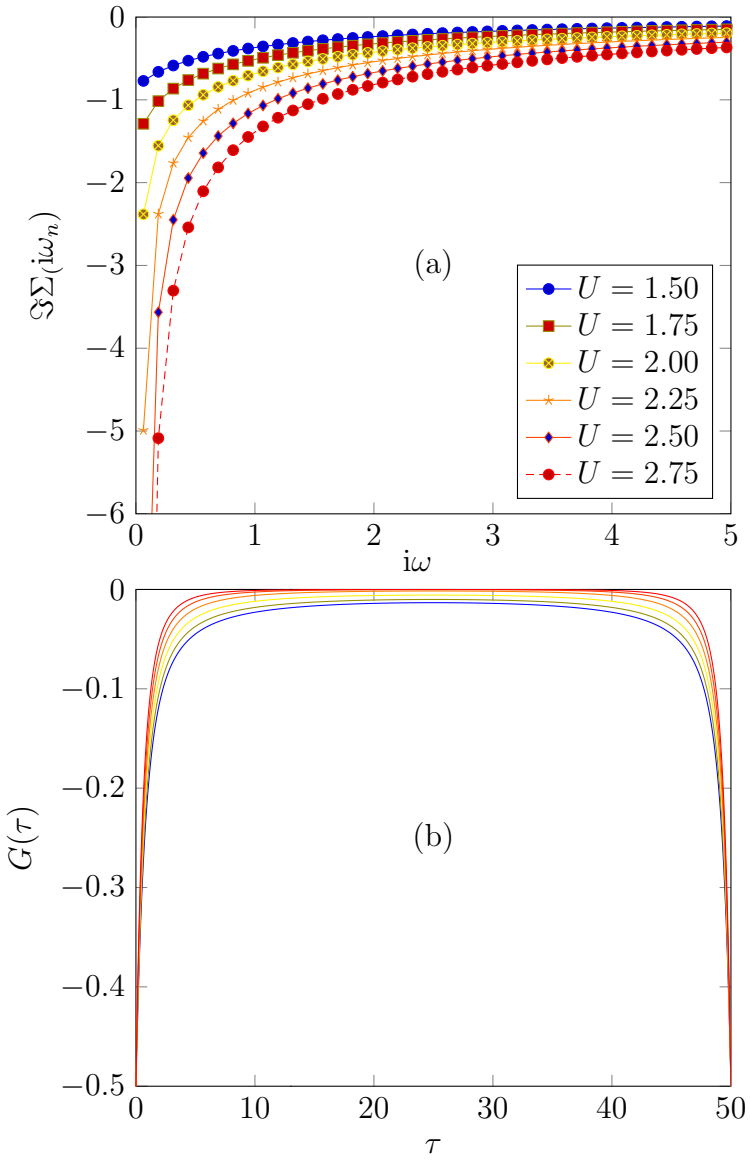

Figure 3.6: (a) The imaginary part of the self-energy in Matsubara frequencies, and (b) the local Green's function in imaginary time for different values of the interaction strength of the temperature independent Mott-like transition on the Bethe lattice in the FK model, which occurs exactly at $U = D = 2$ computed at half-filling for $\beta = 50$, obtained by the code described in Section **??**.

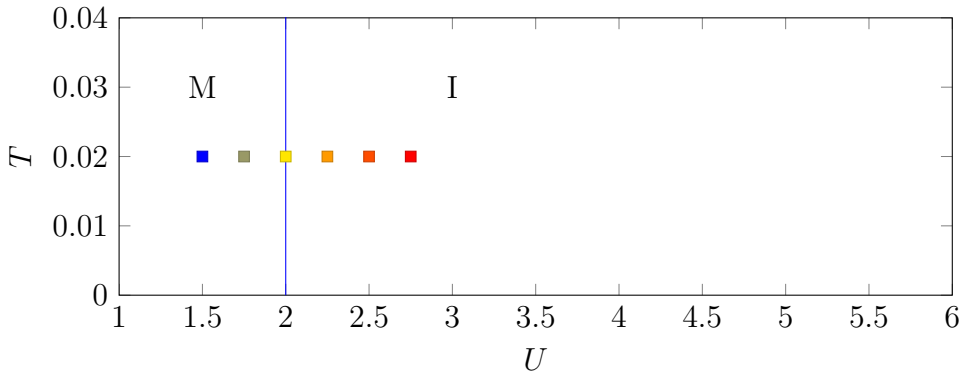

Figure 3.7: The U-T-phase diagramm of the temperature independent Mott-like transition on the Bethe lattice in the FK model, which occurs exactly at $U = D = 2$. The color coded scatter correspond to the solutions shown in Fig. **??**. For $U < D$ the system is metallic (M) and respectively for $U > D$ it is insulating (I).

3.3 w2dynamics

In the standard Hubbard model both spins have equal half bandwidth, $D_1 = D_2$, and hence without any magnetic frustration their solutions are symmetric. In the Bethe-Lattice class of w2dynamics this fact is utilized to suppress Néel order. While in FK-BetheLattice the suppression is achieved by symmetrising the hybridization function in imaginary time. This is necessary as the spin symmetry is lost by spin-dependently choosing the bandwidths. In order to demonstrate the reliability of the results the limit of the standard Hubbard model with $D_1 = D_2$ is discussed. It has the additional advantage of subsequently being able to draw direct comparison for the transition to the FK model. The transition is mimicked by reducing the half bandwidth of one spin D_2, while the half bandwidth of the other spin remains constant, $D_1 = 2$. Fortunately this seems to be the appropriate energy scale.[8]

3.3.1 The standard Hubbard model

Fig. **??** shows the imaginary part of the self-energy and the local Green's function in imaginary time of a system at half-filling with half bandwidths $D_1 = D_2 = 2$ at $\beta = 100$ for different values of the interaction strength close to the Mott transition. For $U = 4.6$ (blue) $U = 4.9$ (yellow) the solution is approached from the atomic limit, i.e. from the insulating phase. For $U = 4.6 < U_{c1}$ (blue) we have only one thermodynamic stable metallic solution which shows proper Fermi liquid like behavior. The case $U = 4.9 > U_{c1}$ (yellow) is insulating, i.e. the imaginary part of its self-energy divergences at $\omega_n = 0$ and $G(\tau = \beta/2)$ is small. Although by approaching that point from the non interacting limit it has a metallic solution, too. The cases $U = 5.2 < U_{c2}$ (orange) and $U = 5.5 > U_{c2}$ (red) are approached from the non interacting limit and analogously show metallic and

[8] One could also think of introducing a mean half bandwidth or a similar effective energy scale.

insulating behavior.

In Fig. **??** the temperature dependency of the Mott transition is shown as a function of interaction strength. The dominant scatter illustrates which solutions have been considered in Fig. **??** and the pale scatter which points have been computed in order to find $U_{c1}(T)$ and $U_{c2}(T)$ (black). Here, the ultimate goal becomes apparent: Connecting the shape of the Mott transition in the Hubbard model on the right hand side, with the infinite straight line on the left hand side, i.e. the Mott-like transition in the FK model, in a meaningful way and ideally understand the meaning.

Before we tackle that problem, let us consider the behavior of the double occupancy and the Z-factor at different temperatures in the standard Hubbard model. In Fig. **??** the hysteresis within the coexistence region of the two quantities is shown at inverse temperatures $\beta = 100$, 50 and 31.25. For temperatures higher than a critical temperatur T_c the solutions pass a cross over region instead of the coexistence region of the Mott transition and the double occupancy as well as the Z-factor are continuous functions, e.g. at $\beta = 20$.

The spectral functions shown in Fig. **??** are obtained by performing MaxEnt on the local Green's function in Matsubara frequencies.[9] For the value of interaction strength $U = 4.6$ (blue) the Hubbard bands are just at the point of separating and the pinned quasi particle peak is developed. For $U = 4.9$ (yellow) the system is within the coexistence region. The solution is approached from the insulating phase and the Hubbard bands are just at the point of rejoining. No quasi particle peak is developed. For $U = 5.2$ (orange) the system is also within the coexistence region. However the solution is approached from the non-interacting limit phase and although the Hubbard bands are already separated, the system is metallic due to the pinned quasi particle peak. For $U = 5.5$ (blue) the Hubbard bands are separated and the quasi particle peak vanished. There is no weight at the chemical potential and hence the system is insulating.

[9] The analytic continuation is done in Matsubara frequencies—instead of imaginary time—because of MaxEnt intrinsic malfunction in case of strong Hubbard band features. The basic problem is over weighting of any central feature of the spectral function. It is discussed in more detail in Ref. **?**.

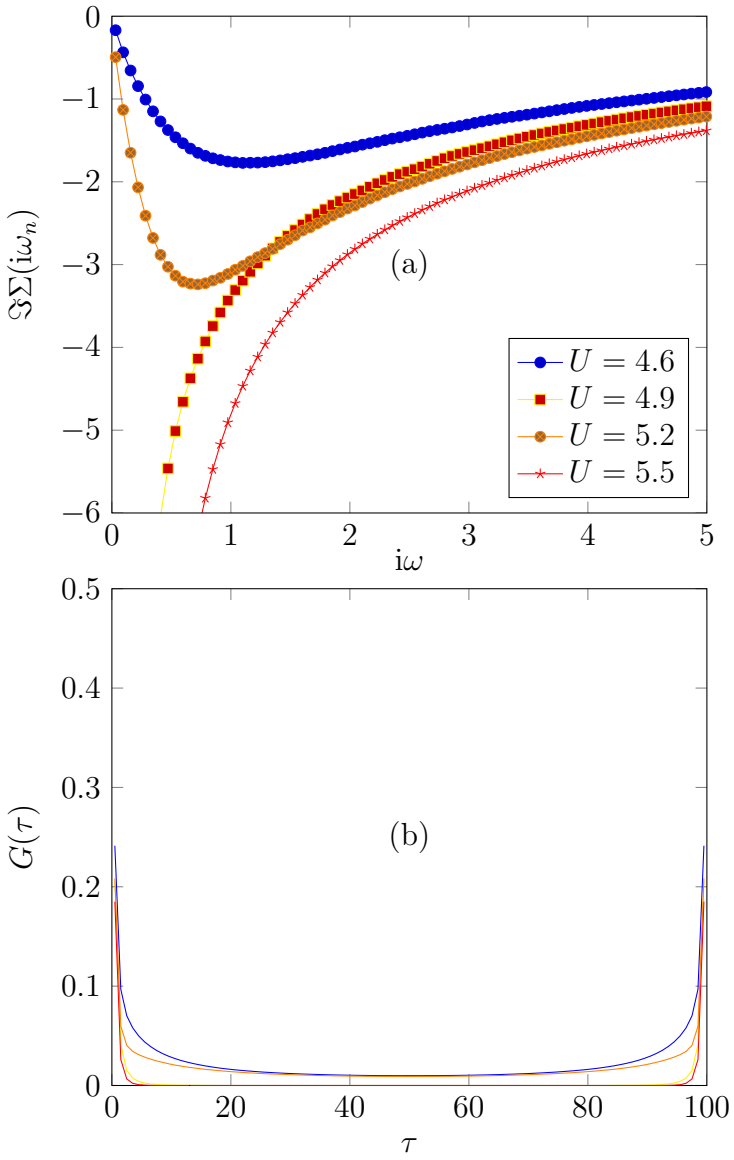

Figure 3.8: (a) The imaginary part of the self-energy in Matsubara frequencies, and (b) the local Green's function in imaginary time for different values of the interaction strength U near the temperature dependent Mott transition on the Bethe lattice in the Hubbard model computed at half-filling at $\beta = 100$ with $D_1 = D_2 = 2$ by the code described in Section **??**.

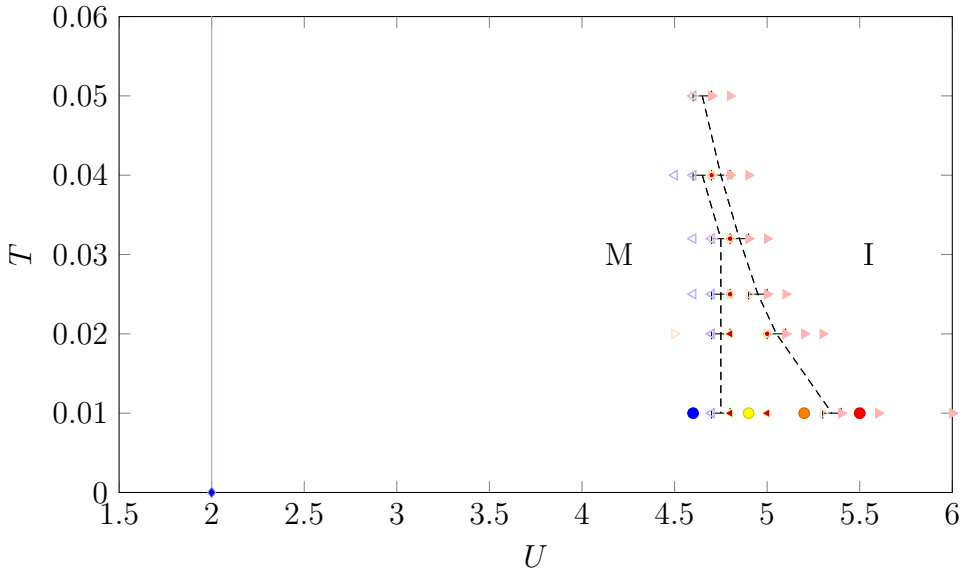

Figure 3.9: The T-U-phase diagram of the Mott transition in the Hubbard model for $D = 2$. The color coded scatter correspond to the solutions shown in Fig. **??**. For $U < U_{c1}$ the system is metallic (M) and for $U > U_{c2}$ insulating (I). The coexistence region is defined within $U_{c1} < U < U_{c2}$. The pale scatter shows which points have been computed: (blue) metallic from insulating, (yellow) insulating from insulating, (orange) metal from metal, (red) insulating from metal. While the pale straight line (blue) indicates the Mott-like transition in the FK model.

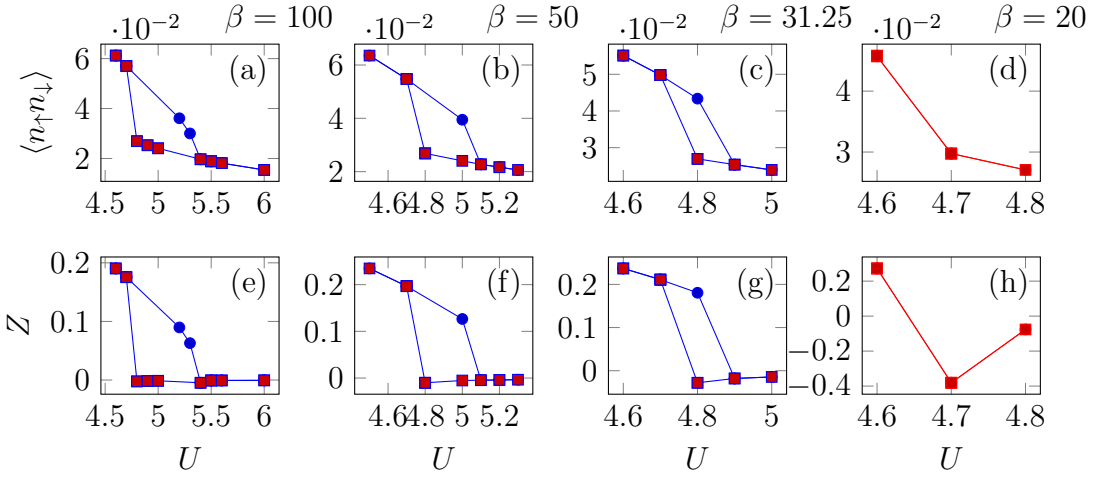

Figure 3.10: The double occupancy $\langle n_\uparrow n_\downarrow \rangle$ (on the top) and the quasi particle residue Z (on the bottom) as a function of the interaction strength U for the temperature dependent Mott transition on the Bethe lattice in the Hubbard model computed at half-filling with $D_1 = D_2 = 2$ at (a), (e) $\beta = 100$ (b), (f) $\beta = 50$ (c), (g) $\beta = 31.25$, and (d), (h) $\beta = 20$

.

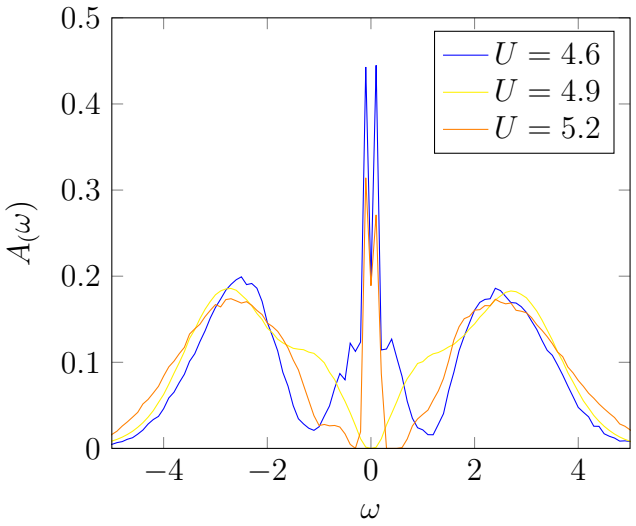

Figure 3.11: Spectral function $A(\omega)$ for different values of the interaction strength U near the temperature dependent Mott transition on the Bethe lattice in the Hubbard model computed at half-filling at $\beta = 100$ with $D_1 = D_2 = 2$ by the code described in Section **??**.

3.3.2 The mass-imbalanced Hubbard model and the transition to the Falicov-Kimball model

The transition of the Hubbard model to the FK model is mimicked by freezing out one spin by making the bandwidth narrower while the other spin remains mobile on the Bethe lattice at half filling. The half-bandwidth of the itinerant spin is set to $D_1 = 2$ which corresponds to a normalized hopping amplitude $t = 1$, while the control parameters are the inverse temperature β, the interaction strength U and the half-bandwidth of the freezing spin D_2.

In Fig. **??** and Fig. **??** (a) - (d) the imaginary part of the self-energy in Matsubara frequencies is compared for a small step towards the FK model, i.e. the half-bandwidths are $D_2 = 1.9$ and 1.95; and a greater step, i.e. $D_2 = 1.15$, at the inverse temperature $\beta = 50$. Fig. **??** and Fig. **??** (e) - (h) display the probability distribution of the expansion order k used by the CT-QMC solver and serve as an indicator for the kinetic energy of each spin. The itinerant spin with $D_1 = 2$ is shown on top and the freezing spin with D_2 on the bottom. The color code is analogous to Fig. **??**, while decreasing D_2 is increasingly pale. For $D_2 = 1.95$ and 1.9 the solutions are computed at the same values of the interaction strength U, while for $D_2 = 1.15$ the Mott transition is significantly shifted and hence the values of the interaction strength are shifted respectively to display solutions across the Mott transition. The considered solutions are highlighted in Fig. **??** (a) by black circles, although the figure is discussed later in more detail.

For the the small step in D_2 the two spins behave very similar. The asymptotic value is dictated by the interaction strength U and is hence the same for $D_2 = 1.95$

and 1.9. For low frequencies the function behaves "more insulating"[10] with decreasing half-bandwidth of the freezing spin. Although the difference is small one observes that for each value of interaction strength the effects are stronger for the itinerant spin. The tendency towards the insulating phase can be understood as a result of the overall decrease of kinetic energy in the system, while the heavier effect on the itinerant spin points towards stronger renormalization for the itinerant spin.

For the bigger step to $D = 1.15$ the difference in behavior of the spins is more obvious. For both spins the asymptotic behavior is shifted according to the shift in interaction strength due to the shift of the Mott transition. In the metallic phase—in Fig. **??**—the freezing spin maintains its quasi particle residue right before the transition occurs, while the renormalization of the itinerant spin is significantly larger.[11] Convolution of the low-frequency and the asymptotic behavior results in a shift of the minimum towards lower frequencies. Extended to the limit of the FK model the minimum gets shifted to $\mathrm{i}\omega_n = 0$. The quasi particle residue of the itinerant spin goes to zero, $Z \to 0$, which may be caused by an attempt of the system to compensate the mismatch in the kinetic energy of the itinerant spin and the completely frozen spin. It results in a behavior as shown in Fig. **??** (a) for the values $U = 1.5$ and 1.75 of the interaction strength. Lastly, the process of freezing generally has less impact on the insulating solution, which is likely due to less overall movement in the system. The overall tendency towards the insulating phase is further supported by the changes of the local Green's function in imaginary time. However it is not discussed—neither shown—as there are no further conclusions drawn by it.

The shift of the Mott transition is investigated by performing two cuts at constant temperature, at $\beta = 50$ and $\beta = 100$, as shown in Fig. **??**. The critical interaction strength as a function of the half-bandwidth of the freezing spin, $U_{c1}(D_2)$ and $U_{c2}(D_2)$, show almost linear behavior seemingly to intersect the U-axis—for $D_2 = 0$—at $U = 2$. Furthermore the coexistence region is smaller towards narrower bandwidths as emphasized in Fig. **??**. The result is perfectly in agreement with the FK model with $D_2 = 0$, where the Mott-like transition takes place at $U = D_1 = 2$ without coexistence region.

In Fig. **??** the quasi particle residue Z is shown for different bandwidths, $D_2 = 2$, 1.6, 1.2, 0.8 and 0.4, at $\beta = 100$—on the left hand side—and $\beta = 50$—on the right hand side—for the itinerant and the freezing spin.[12] The itinerant spin with D_2 gets heavier, while the coexistence region gets narrower and is shifted towards lower interaction strength. Interestingly for a constant value of D_2 the height of the hysteresis curve depends on the spin, but not its width. It suggests that even though the spins are renor-

[10] The absolute value of the slope as well as the minimum value of the self energy for metallic solutions increases, while insulating solutions tend towards earlier divergence.

[11] This suggests that the system always becomes insulating as soon as both spins, i.e. all electrons, get heavier than a certain critical effective mass. Furthermore the system may aim for the same effective kinetic energy of both spins. Therefore the already heavier spin—i.e. the freezing spin—needs less renormalization.

[12] $(D_2,\beta) = (0.4,50)$ is excluded as it is bad data. The coexistence region is very narrow at that point and therefore the solutions easily slip into the insulating phase within the error bars. Furthermore, quantum Monte Carlo integration suffers from critical slowing-down in the vicinity of a critical point, which causes results to be less reliable.

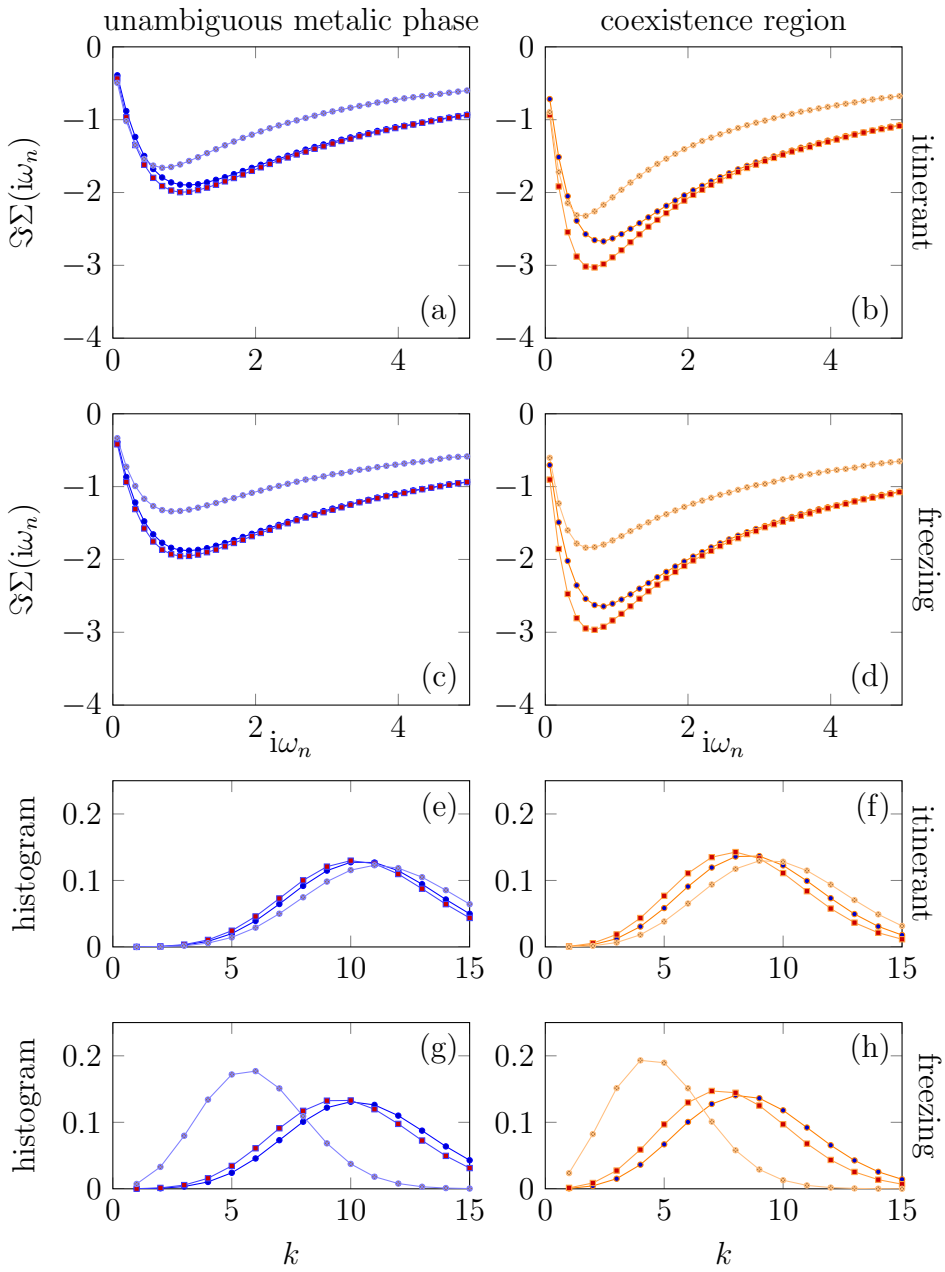

Figure 3.12: (a) - (d) Imaginary part of the self-energy in Matsubara frequencies, (e) - (h) Histogram of the expansion order k in the CT-QMC,
for different values of the interaction strength U in the metallic phase near the Mott transition on the Bethe lattice in transition of the Hubbard model to the FK model computed at half-filling at $\beta = 50$ with $D_1 = 2$ for the itinerant spin—(a), (b), (e) and (f)—by the code described in Section **??**. A comparison of different half bandwidths D_2 of the freezing spin—(c), (d), (g) and (h): A comparison of different spin—(c), (d), (g) and (h): Just at the point of entering the coexistence region with (U,D_2): $(4.6, 1.95)$ **??** $(4.6, 1.9)$ **??** $(3.6, 1.15)$ **??** and within the coexistence region with $(4.9, 1.95)$ **??** $(4.9, 1.9)$ **??** $(3.8, 1.15)$ **??**.

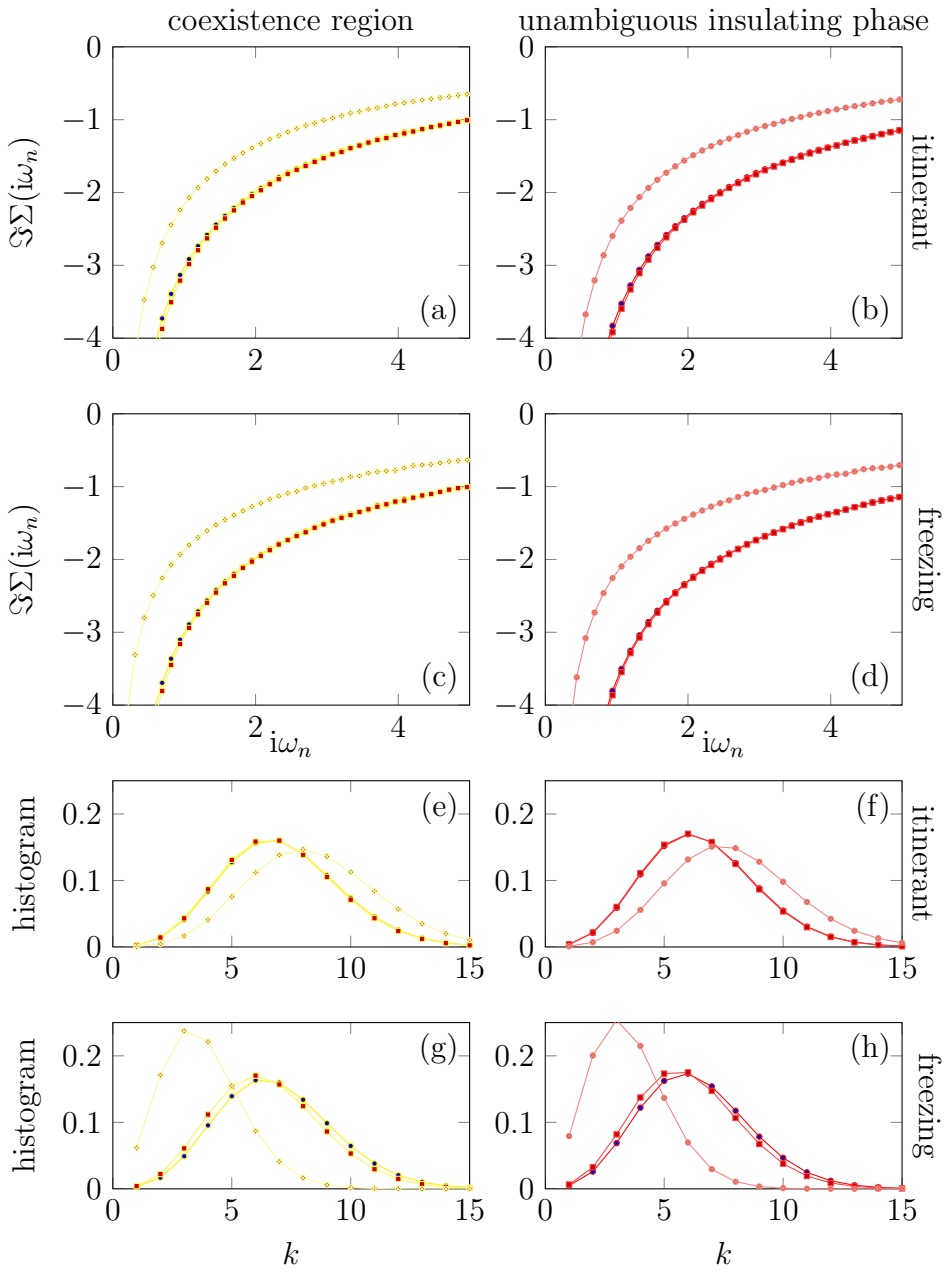

Figure 3.13: (a) - (d) Imaginary part of the self-energy in Matsubara frequencies, (e) - (h) Histogram of the expansion order k in the CT-QMC,
for different values of the interaction strength U in the insulating phase near the Mott transition on the Bethe lattice in transition of the Hubbard model to the FK model computed at half-filling at $\beta = 50$ with $D_1 = 2$ for the itinerant spin—(a), (b), (e) and (f)—by the code described in Section **??**. A comparison of different half bandwidths D_2 of the freezing spin—(c), (d), (g) and (h): Within the coexistence region with (U, D_2): $(4.7, 1.95)$ **??** $(4.7, 1.9)$ **??** $(3.7, 1.15)$ **??**, and before entering the coexistence region with $(5.0, 1.95)$ **??** $(5.0, 1.9)$ **??** $(3.9, 1.15)$ **??**.

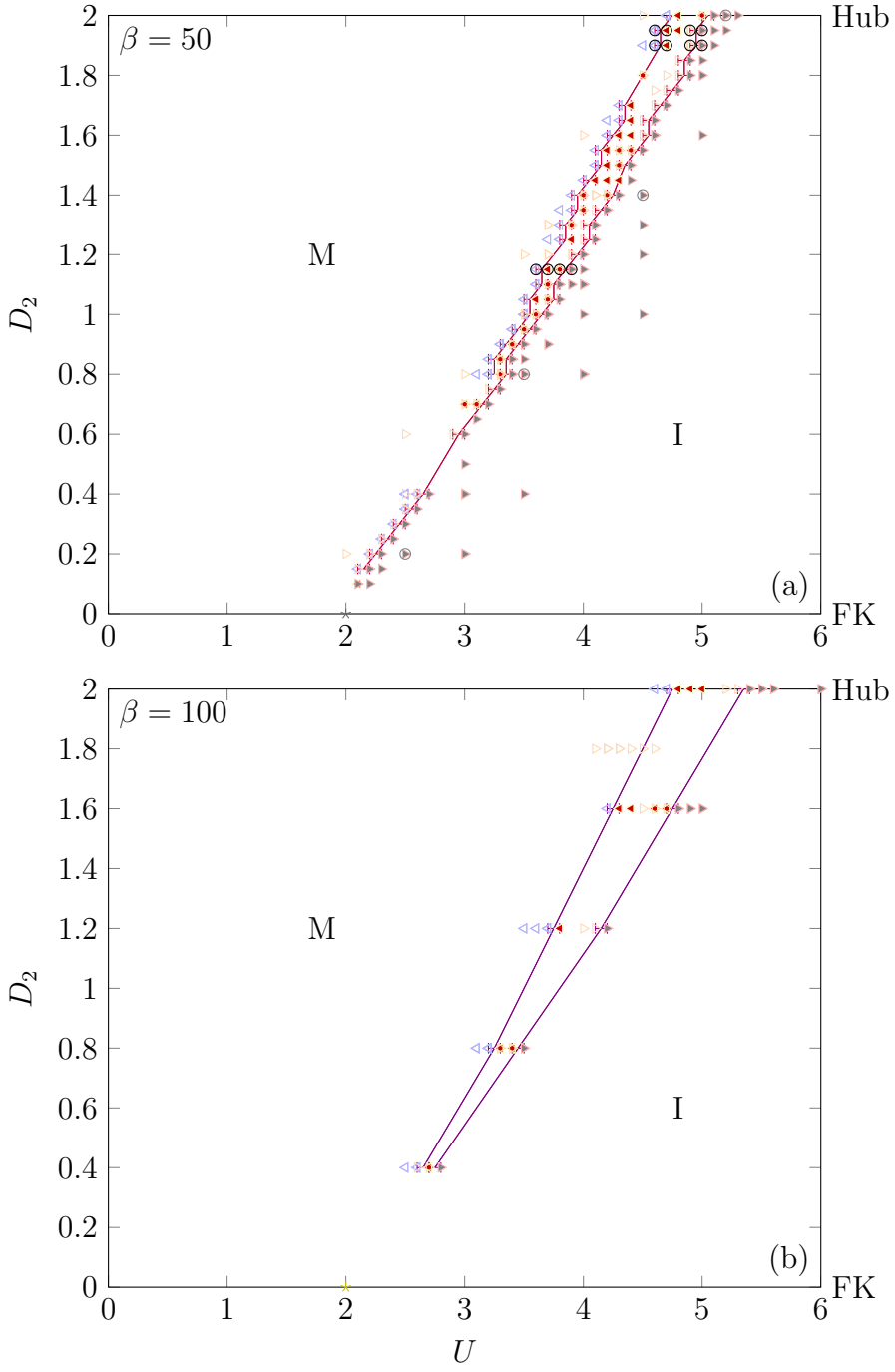

Figure 3.14: The U-D_2-phase diagram of the Mott transition for the transition of the Hubbard model towards the FK model for $D_1 = 2$ on the Bethe lattice at inverse temperature (a) $\beta = 50$, and (b) $\beta = 100$.

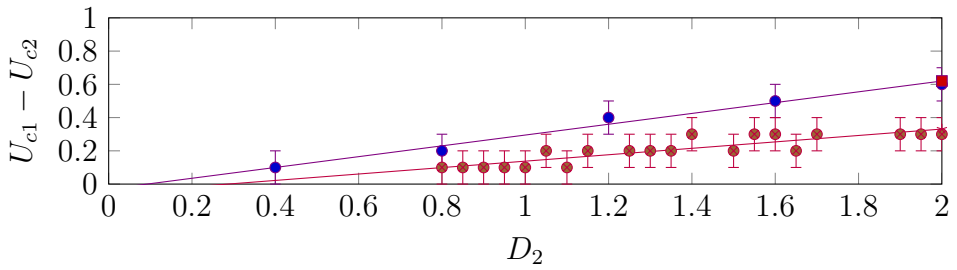

Figure 3.15: The width ot the coexistence region $U_{c1} - U_{c2}$ of the Mott transition as a function of the half-bandwidth of the freezing spin D_2 for the transition of the Hubbard model towards the FK model for $D_1 = 2$ on the Bethe lattice at inverse temperature **??** $\beta = 50$, and **??** $\beta = 100$.

malized differently, the phase transition, i.e. the limits of the coexistence region, are the same (at least up until $D_2 = 0.4$ for $D_1 = 2$).[13] The interpretation is consistent with the change observed in the imaginary part of the self-energy in Matsubara frequencies.[14]

In Fig. **??** the ratio of the quasiparticle residues of the two spins is shown for different half-bandwidth of the freezing spin D_2. The data points towards a constant ratio for each ratio of the half-bandwidths, $\frac{Z_1}{Z_2} \propto \frac{D_2}{D_1}$ suggesting $D_1 Z_1 = D_2 Z_2 = const.$. A possible explanation can be reasoned as follows: Considering a system with spin 1 and 2, with the kinetic energy

$$E_1 = \frac{p_1^2}{2m} \qquad \text{and} \qquad E_2 = \frac{p_2^2}{2m}. \tag{3.5}$$

The kinetic energy of a spin is generally proportional to its bandwidth, $E_i \propto D_i$. Here the assumption is made that in a wide range[15] around the Mott transition the system aims for a spin-independent effective kinetic energy,

$$E^* = \frac{p_1^2}{2m_1^*} = \frac{p_2^2}{2m_2^*}, \tag{3.6}$$

as reasoned in Footnote **??**. By recalling Eq.(**??**),

$$\underbrace{\frac{p_1^2}{2m}}_{\propto D_1} Z_1 = \underbrace{\frac{p_2^2}{2m}}_{\propto D_2} Z_2 \tag{3.7}$$

[13] The statement is unexpected in the sense that in the FK model the frozen spin is never in the metallic phase. Hence one could expect the transition of the freezing spin to wander of to $U = 0$ and $D_2 = 0$ at some point.

[14] Reminder: While the itinerant spin gets renormalized more heavily the freezing spin maintains its Z-factor right next to the critical interaction strength $U_{c1}(D_2)$ and $U_{c2}(D_2)$. These critical values of divergence are spin-independent.

[15] It is clear that for $U = 0 : Z_1 = Z_2 = 1$. Thus it would be interesting to have a closer look at this assumption by investigating the ratio Z_1/Z_2 for small values of U, analog to the analysis in Fig. **??** in the range of the Mott transition.

is obtained and hence

$$\frac{D_1}{D_2} \propto \frac{Z_2}{Z_1}. \tag{3.8}$$

In Fig. **??** the difference of the quasiparticle residue of the two spins is shown as a function of the interaction strength, $Z_1 - Z_2(U)$, for different half-bandwidth of the freezing spin D_2. The function can be described by[16]

$$Z_1 - Z_2(U; D_2) = a(D_2)\left(U + b(D_2)\right)^2 + c(D_2), \tag{3.9}$$

where $a(D_2)$, $b(D_2)$ and $c(D_2)$ are fitting parameters.[17] The coexistence region ends when the function gets zero, i.e. $Z_1 - Z_2(U_{c2}) = 0$, since the quasi particle residue—which is actually not defined in the insulating phase—can be thought of as $Z \to 0$ in the Brinkman-Rice picture of the Mott transition.[18]

The shrinking coexistence region in the U-D_2-phase diagram in Fig. **??** does not fully characterize the transition of the Mott transition of the Hubbard model to the FK model. Suppose the coexistence region gets smaller as a function of D_2 for all temperatures and vanishes only at $D_2 = 0$. This behavior would connect the critical temperature T_c of the Mott transition in the Hubbard model to a point on a temperature-independent straight line—i.e. the Mott-like transition in the FK model—in Fig. **??**. From the point of view of the FK model the value T_c of the Hubbard model is arbitrary so that—motivated by Renormalization Group—two guesses arise: Either the critical temperature decreases as some function of freezing one spin vanishing at $D_2 = 0$ or the critical temperature increases as a function of reducing D_2 going to infinity at $D_2 = 0$.

In order to investigate these hypothesis a cut at constant bandwidth with $D_2 = 1.6$ is evaluated as shown in Fig. **??**. The shift in the interaction strength as well as narrowing is observed—c.f. values at $\beta = 100$ and $\beta = 25$. However the resolution is too poor in order to make predictions about the critical temperature. It is partly due to the effect of critical slowing-down in quantum Monte Carlo methods near the critical point.

A comparison of the hysteresis of the double occupancy at different temperatures with $D_2 = 1.6$ to the standard Hubbard model—as shown in Fig. **??**—points towards T_c being a trivial function of D_2, $T_c(D_2) = \text{const}$. The hysteresis are merely shifted while the slopes do not significantly change. Although the change may just be too small for observation.

Therefore the significance in the change of the hysteresis in the double occupancy is considered when varying the half-bandwidth of the freezing spin D_2 at constant temperatures, $\beta = 100$ and $\beta = 50$, in Fig. **??**. Even though the step-size of D_2 is constant, $\Delta D_2 = 0.4$, the change is increasing.[19] It supports the assumption that at some critical half-bandwidth of the freezing spin $D_{c2}(T)$ the coexistence region vanishes,

[16] I also plotted the the data over U^2 and found a straight line. The point of this plot is that there may be a (phenomenological) possibility to make precise predictions about where to find the MIT and coexistence region for arbitrary D_2.

[17] These parameters should be determined by a fitting procedure. It seems like there is some sort of exponential or $1/U$ envelope function involved.

[18] Possibly the coexistence region is entered when the parabola and the envelop function are touching.

[19] It seems to be quadratic in relation to the increasing relative change.

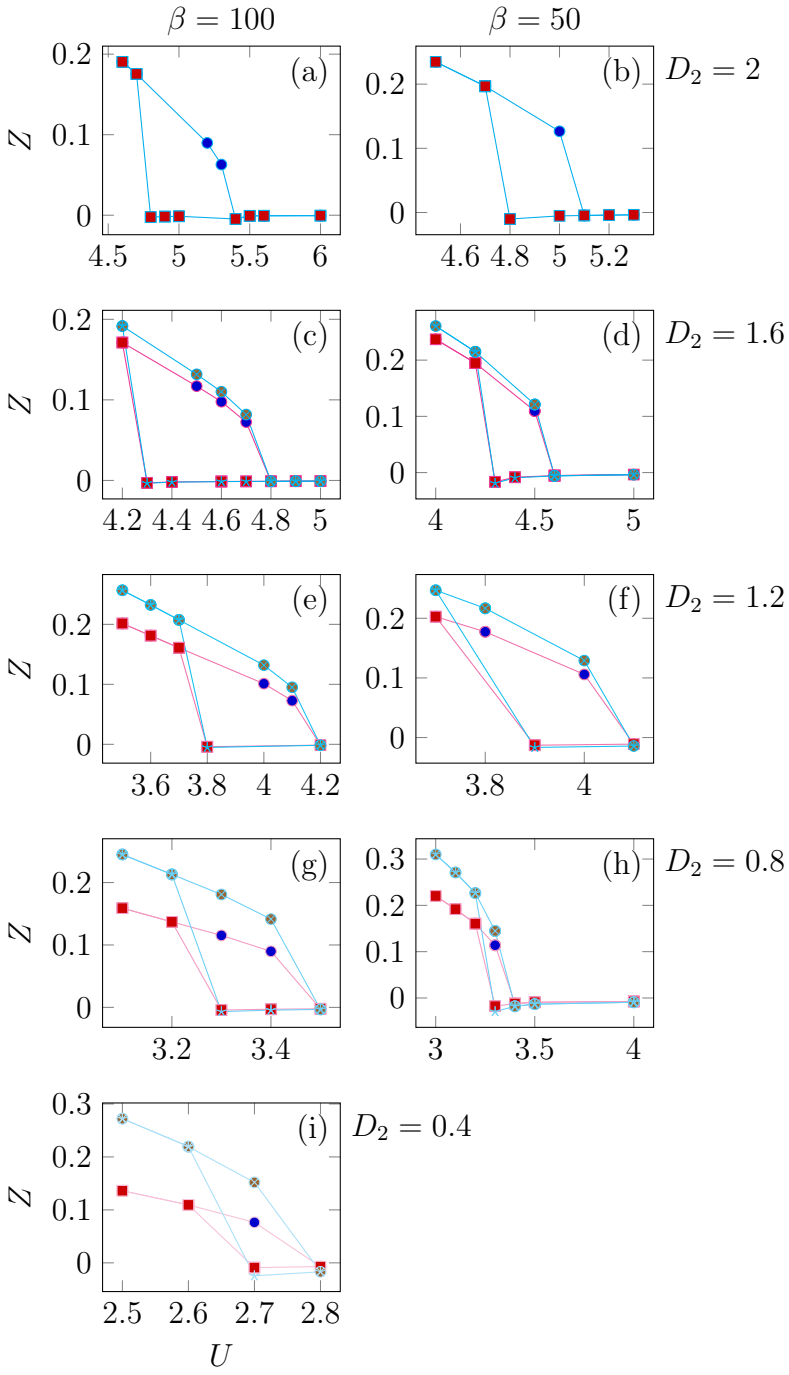

Figure 3.16: The spin dependent quasi particle residue Z as a function of the interaction strength U in the range of the Mott transition for the half-bandwidth of the itinerant spin **??** $D_1 = 2$ and at different values of the bandwidth of the freezing spin D_2 at $\beta = 100$ on the left hand side and at $\beta = 50$ on the right hand side for the half-bandwidth of the freezing spin **??** (a), (b) $D_2 = 2$, (c), (d) $D_2 = 1.6$, (e) $D_2 = 1.2$ (f) $D_2 = 1.25$, (g), (h) $D_2 = 0.8$, (i) $D_2 = 0.4$

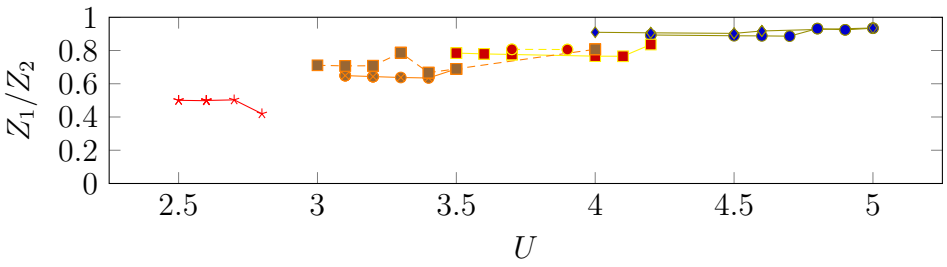

Figure 3.17: Ratio of the quasiparticle residues of the two spins as a function of the interaction strength U for the temperature dependent Mott transition on the Bethe lattice at half-filling for the transition of the Hubbard model towards the FK model at $\beta = 100$ and $\beta = 50$, with $D_1 = 2$ and (olive) $D_2 = 1.6$, (yellow) $D_2 = 1.2$, (orange) $D_2 = 0.8$, (red) $D_2 = 0.4$.

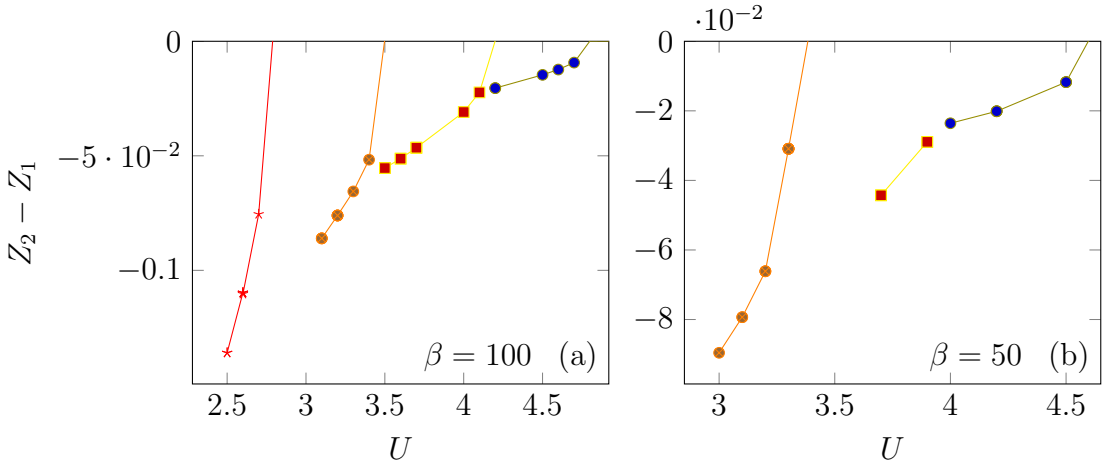

Figure 3.18: The difference of the quasi particle residues of the two spins as a function of the interaction strength U for the temperature dependent Mott transition on the Bethe lattice computed at half-filling in the transition of the Hubbard model (blue) towards the FK model at $\beta = 100$ and $\beta = 50$, with $D_1 = 2$ and (olive) $D_2 = 1.6$, (yellow) $D_2 = 1.2$, (orange) $D_2 = 0.8$, (red) $D_2 = 0.4$.

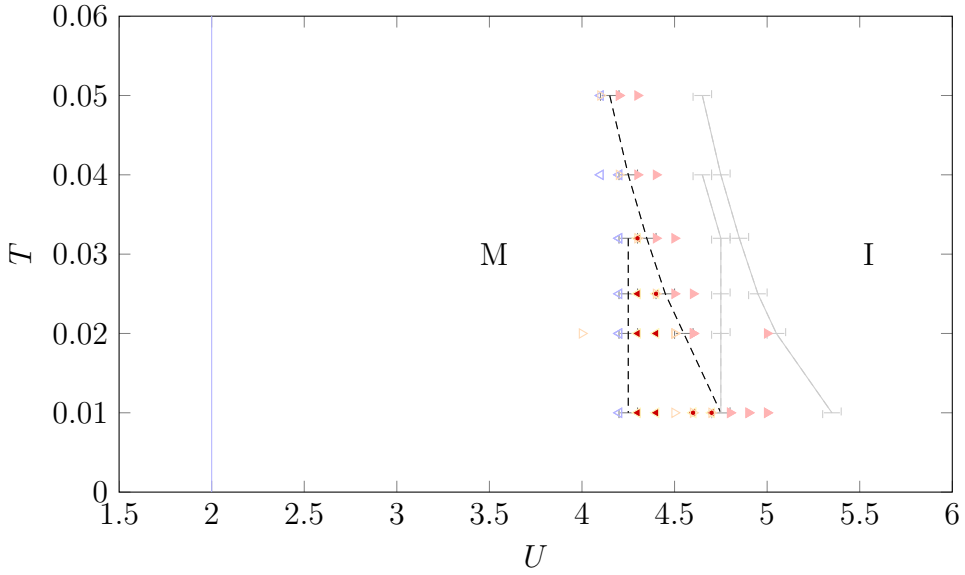

Figure 3.19: U-T-phase diagram of the first order Mott transition with $D_1 = 2$ and $D_2 = 1.6$ on the Bethe lattice. For $U < U_{c1}$ the system is metallic (M) and for $U > U_{c2}$ insulating (I). The coexistence region is defined within $U_{c1} < U < U_{c2}$. The pale scatter illustrate which points have been computed: (blue) metallic from insulating, (yellow) insulating from insulating, (orange) metal from metal, (red) insulating from metal. The pale straight line (blue) indicates the Mott-like transition in the FK model, while the pale gray lines indicate the Mott transition in the Hubbard model.

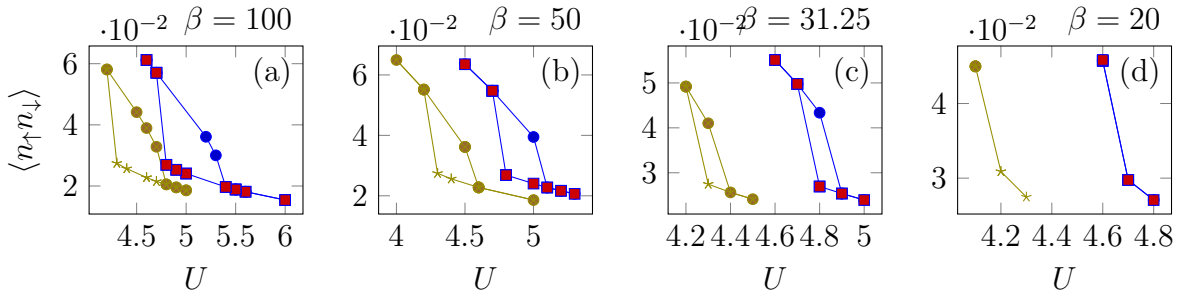

Figure 3.20: Double occupancy $\langle n_\uparrow n_\downarrow \rangle$ as a function of the interaction strength U for the temperature dependent Mott transition on the Bethe lattice in the Hubbard model with $D_1 = D_2 = 2$ (pale) and close to the Hubbard model with $D_1 = 2$ and $D_2 = 1.6$ computed at half-filling at (a) $\beta = 100$, (b) $\beta = 50$, (c) $\beta = 31.25$, and (b) $\beta = 20$.

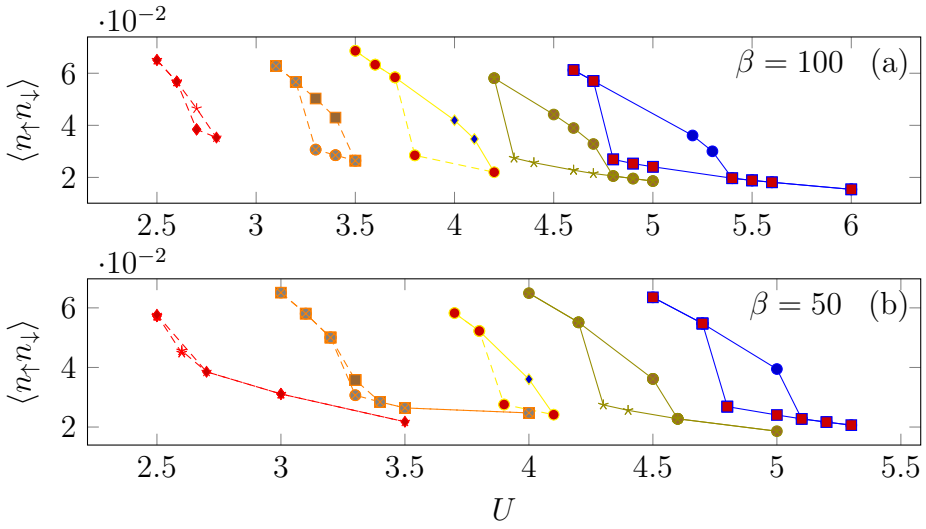

Figure 3.21: The double occupancy $\langle n_\uparrow n_\downarrow \rangle$ as a function of the interaction strength U for the temperature dependent Mott transition on the Bethe lattice computed at half-filling in the transition of the Hubbard model (blue) towards the FK model at (a) $\beta = 100$, (b) $\beta = 50$, with $D_1 = 2$ and (blue) $D_2 = 2$, (olive) $D_2 = 1.6$, (yellow) $D_2 = 1.2$, (orange) $D_2 = 0.8$, (red) $D_2 = 0.4$.

$U_{c1} - U_{c2}(D_{c2}(T)) \equiv 0$.[20] $D_{c2}(T)$ could still equal zero for all temperatures that feature a coexistence region in the Hubbard model, though. The only hint that $D_{c2}(T)$ increases for lower temperatures, or rather $T_c(D_2)$ goes to zero for the FK model, is given in Fig. **??**. The linear regression of the width of the coexistence region $U_{c1} - U_{c2}(D_2)$ at $\beta = 100$ is equal zero for finite $D_{c2}(\beta = 100)$ and smaller than $D_{c2}(\beta = 50)$, $0 < D_{c2}(\beta = 100) < D_{c2}(\beta = 50)$.[21]

The spectral function $A(\omega)$ is shifted in its behavior respectively to the Mott transition, see Fig. **??**. The Hubbard bands remain centered at values of frequency half of the interaction strength, $\omega = U/2$ as known from the standard Hubbard model. Interestingly, the low-frequency spectral weight seems to be less significantly shifted compared to the high frequency weight. It results in the impression that the Hubbard bands consist of two independently moving peaks: The main peak and a smaller low-frequency peak.

The low-frequency peak has been referred to as MaxEnt resonance peak as it has already been seen in the standard Hubbard model. However no physical interpretation is known. Fig. **??** shows insulating spectral functions of the same relative distance to the Mott transition in the U-D_2-phase diagram highlighted by gray circles in Fig. **??** (a). The spectra feature fixed lower frequency peaks, while the main peaks drift apart

[20] T_c does not seem to go to ∞ otherwise the change in $\beta = 50$ would likely be slower than in $\beta = 100$. Although, here, the speed of change relies merely on impression.

[21] This result is obtained by assuming linear behavior. Linearity seems to be appropriate, however the physical understanding of why the sudden asymmetry and a change of kinetic energy would result in a linear behavior is not given.

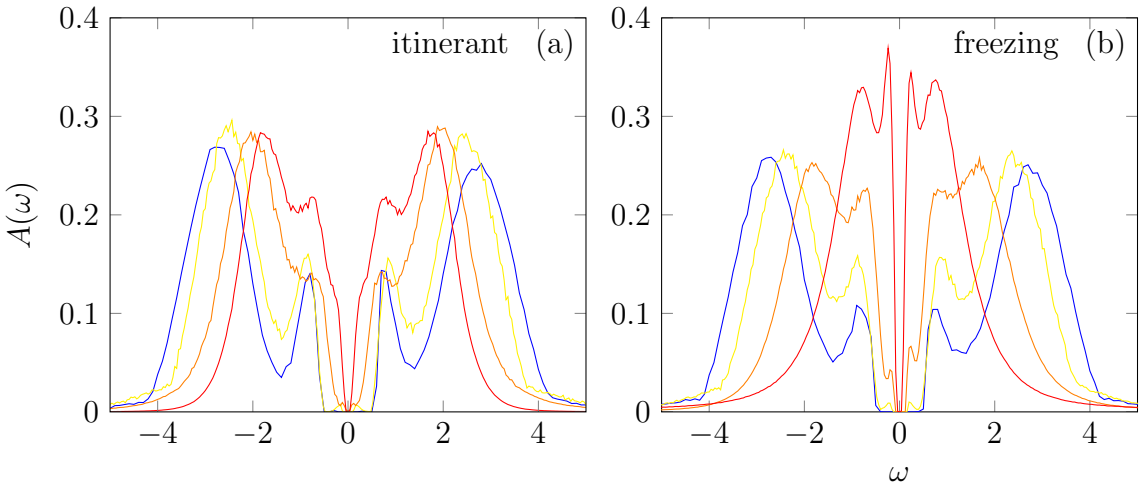

Figure 3.22: The spectral function $A(\omega)$ for different values of interaction strength U in the insulating phase near the Mott transition on the Bethe lattice in transition of the Hubbard model to the FK model computed at half-filling at $\beta = 50$ with $D_1 = 2$ for (a) the itinerant spin and (b) the freezing spin with (D_2, U): **??** (5.2,2.0), **??** (4.5,1.4), **??** (3.5,0.8), and **??** (2.5,0.2) by the code described in Section **??**.

as dictated by $U/2$. Although the pseudo gap separating the two peaks is likely to be overestimated by MaxEnt as one can see from the results in Ref. **?**, the spectra are evidence of a hidden energy scale within the system. It is similar to the fact that the quasi particle residue of the freezing spin D_2 right before entering the coexistence region is equal for different half-bandwidth. The movement of the main peak might be coupled to the effective kinetic energy of the system while the low-frequency peak is coupled to the behavior of a spin-dependent value such as its kinetic energy. Analogous to the case where both spins must be heavier than a certain critical effective mass, in the end maybe only one spin determines the behavior of the low-frequency peak. The burning question is which parameter is constant for the chosen D_2 and U values in the insulating phase. The quasi particle residue is not defined and from Fig. **??** it does not seem to be the double occupancy either.

4 Conclusion and Outlook

In the scope of this thesis the metamorphosis of the Hubbard model to the FK model is analyzed by means of the Mott transition in a fermionic system on the Bethe lattice in infinite dimensions. Therefore code is implemented that allows a spin-independent choice of the half-bandwidth of the Bethe DOS. It is accompanied by a new way of suppressing Néel order by exploiting symmetries of the hybridization between the impurity and the bath states.

When the half-bandwidth of one spin is reduced, while the half-bandwidth of th other spin stays constant, we observe some basic changes:

- The Mott transition is shifted linearly to occur at lower interaction strength.
- The width of the coexistence region—defined by the difference of the critical interaction strength—is getting smaller.
- The height of the coexistence region—referring to the critical temperature—is probably reduced.
- The double occupancy of a site gets less likely.
- The itinerant spin gets renormalized more heavily as compared to the freezing spin.
- In the spectral function of the insulating phase the Hubbard bands split up in 2 independently moving peaks. The main peak is centered at $\pm U/2$, while the side peak remains at constant position for equal distance to the Mott transition.

The change in behavior is driven by two concepts. The total kinetic energy $E_1 + E_2$ of the electrons and the mismatch or respectively the ratio of the kinetic energy of the spins E_1/E_2. A possible explanation for the observations can be given with the following physical processes and assumptions:

- The system renormalizes both spins so that they exhibit the same effective kinetic energy.
- The freezing spin undergoes stronger localization effects as the itinerant spin.
- The system has less total kinetic energy.
- Some critical values must be passed by both spins while some need only one.

- The Kondo effect is most likely to occur for spins with velocity of the same order of magnitude.

Thereby some arguments can be made:

The freezing electrons are moving slower as they have less kinetic energy compared to the itinerant spins. In order to obtain the same effective kinetic energy the freezing spin has a lighter effective mass compared to the itinerant spin. Or equivalently the itinerant spin gets renormalized more heavily.

The linear decrease of the total kinetic energy is narrowing the Hubbard bands linearly. It causes the Mott transition to be shifted towards smaller interaction strength almost linearly. The shift is slightly slower closer to the Hubbard model, i.e. for smaller mismatch in the kinetic energy, due to another effect: The Hubbard bands are additionally narrowed by the main peak and the low-frequency peak merging. Trying to make an educated guess, the position of the side peak is due to the kinetic energy of one spin.[1] The underlying process may depend on the localization of the freezing spin.

The Mott transition is driven by the quasiparticle residue of the freezing spin. Or equivalently, only when both spins are heavier than some spin-dependent critical effective mass the system becomes insulating, and hence vice versa when one spin is lighter than some other critical effective mass the system is metallic. It makes more sense of why the critical interaction strengths decreases linearly as a function of the half-bandwidth of the freezing spin, but additionally of the shrinking coexistence region. Following the argument of the system aiming for equal effective kinetic energy: In the limit of the FK model the itinerant spin is infinitely faster than the frozen one causing a infinitely stronger renormalization of the itinerant spin decreasing the correlation temperature. The Mott-like transition in the FK model describes physics infinitely high above the Mott transition in the Hubbard model. It also allows the statement that the quasiparticle concept holds just as much as it does for the Hubbard model at high temperatures where the life-time is infinitely short.

The tendency of the freezing spin towards localization is observed by the decrease of the double occupancy for decreasing values of the half-bandwidth of the freezing spin at constant interaction strength. It might be caused by the itinerant spin being faster to react on a site being occupied while the freezing spin is slower in changing the site. It results in the electrons to less likely occupy the same site.

The Kondo temperature may behave in a way that the heavier itinerant spin determines the likelihood of the Kondo effect. So the stronger renormalized spin determines the Kondo temperature that in turn determines the width of the quasi particle peak. It causes the coexistence region to shrink for a greater mismatch in the kinetic energy. On the other hand it may be that the Kondo effect is just more likely for spins that have the same magnitude of velocity and hence the coexistence region vanishes. However the shrinking should then be slower for higher temperatures, i.e. for systems with more smearing in the energy scales. Also it would imply that they have to sit together for a long time on the same site to do the spin flip. But at the Mott transition close to the

[1] Probably due to the kinetic energy of the freezing spin as it also determines the position of the Mott transition.

FK model the double occupancy of the insulating state is higher than the one close to the Hubbard model of the metallic state.

Although we gained a greater understanding of how the metamorphosis takes place there are plenty of questions that remain unanswered are:

- Why is the coexistence really region shrinking?
- What causes the low-frequency peaks?
- Can we make predictions about the coexistence region by a better understanding of the spin-dependent quasiparticle residue as a function of the half-bandwidth and the interaction strength?
- And lastly what about two particle quantities?

Appendices

A code

A.1 bethe-phasediagram-14-04-15.py

```
# bethe-phasediagram-14-04-15.py
# Marie-Therese Philipp
# Calculates the local Green's function in imaginary time
# and the self-energy in Matsubara frequencies
# of the Bethe lattice in the FK model
# for different values of interaction strength.
# The data is ploted and stored in txt files.

# Parameters.in
#########################################################
#[General]
#DOS = Bethe
#half-bandwidth = 1
D=2 + 0.j
#mu =
beta = 50.0
#NAt = 1
DMFTsteps = 20
FileNamePrefix = "FK-bethe"
#readold = 0

#[QMC]

#Eigenbasis = 1
#NCorr = 10
#Nmeas = 1e6
#Nwarmups = 1e6
Ntau = 1000
Niw = 200

#truncation = 2

#########################################################

U_min = 1.5          # minimal interaction energy if fixed electron is
    present
U_step= 0.25          #
Usteps= 5            # how many times U_step is added
p = 0.5              # occupation probability

#########################################################
```

```
import numpy as np
import matplotlib.pyplot as pl
from matplotlib2tikz import save as tikz_save

def Green_local(z, fiw, U=0., p=0.5, mu=0):
    return p / ( z-fiw-U+mu ) + (1-p) / ( z-fiw+mu )

def Green_bare(z, fiw, mu=0):
    x = (1j*w-fiw[0]+mu).imag
    return 1./ (1j*x)

def dyson_siw( G, G0 ):
    return 1./G0 - 1./G

def Green_local_analytically(z, d, siw, mu=0 ):
    zeta = (1j*w-siw[0]+mu).imag
    return 2*(1j*zeta)/d**2*( 1 - np.sqrt( 1 - d**2/(1j*zeta)**2 ) )

def hybridization(z, gloc, siw, mu=0):
    x = (1j*w-siw[0]+mu).imag
    return (1j*x) - 1./gloc

def FT(z, Aiw, tau, beta):
    return 1./beta*np.sum(np.exp(-z[0,:,np.newaxis]*tau[np.newaxis
        ,:])*Aiw[0,:,np.newaxis]+np.exp(z[0,:,np.newaxis]*tau[np.
        newaxis,:])*np.conjugate(Aiw[0,:,np.newaxis]), axis=0)


##########################################################

w = np.fromfunction(lambda i, j: np.pi*(2*j+1)/beta + 0.j, (1,Niw) )
tau = np.linspace(0, beta, Ntau)

U_list_gloc =[]
U_list_giw =[]
U_list_siw=[]
U_list_glocold =[]
U_list_fiw=[]
U_list_gtau=[]

U_loop_cnt=0
U = U_min
mu = U_min/2
while U_loop_cnt<Usteps+1:

    siw = np.zeros( (1,np.size(w)) )

    first_gloc= Green_local_analytically( (1j*w), D, siw, mu )

    fiw = hybridization( (1j*w), first_gloc, siw, mu)

    list_gloc =[first_gloc]
```

```
list_giw =[]
list_siw=[]
list_glocold =[]
list_fiw=[fiw]
list_gtau=[ FT(1j*w,first_gloc,tau,beta) ]

loop_cnt=0
while loop_cnt<DMFTsteps:

    glocold = Green_local( (1j*w), fiw, U, p, mu )

    giw = Green_bare( (1j*w), fiw, mu)

    siw = dyson_siw( glocold, giw )

    gloc= Green_local_analytically( (1j*w), D, siw, mu )

    gtau= FT(1j*w,gloc-1/(1j*w),tau,beta)- 0.5

    fiw = hybridization(1j*w, gloc, siw, mu)

    list_gloc.append(gloc)
    list_siw.append(siw)
    list_giw.append(giw)
    list_glocold.append(glocold)
    list_fiw.append(fiw)
    list_gtau.append(gtau)
    del glocold
    del giw
    del siw
    del gloc
    del gtau
    loop_cnt+=1
del loop_cnt

U_list_gloc.append(list_gloc[DMFTsteps-1][0])
U_list_siw.append(list_siw[DMFTsteps-1][0])
U_list_giw.append(list_giw[DMFTsteps-1][0])
U_list_glocold.append(list_glocold[DMFTsteps-1][0])
U_list_fiw.append(list_fiw[DMFTsteps-1][0])
U_list_gtau.append(list_gtau[DMFTsteps-1])
del list_gloc
del list_siw
del list_giw
del list_glocold
del list_fiw
del list_gtau

U_loop_cnt+=1
U += U_step
del mu
mu = U/2
```

```
############################################################

print "\nDMFTsteps = " +str(DMFTsteps)
print "U = [" +str(U_min) +";"+ str(U_min+U_step*Usteps)+"]"
print "1/T = "+str(beta.real)
print "half filling\n"

for i in range(0, Usteps+1):
    filename = FileNamePrefix + "_gtau_U=" + str(U_min+i*U_step)
    tau_gtau = np.array( (tau.real,U_list_gtau[i].real) )
    tau_gtau = np.reshape( tau_gtau, (2*np.size(tau)), order='F')
    tau_gtau = np.reshape( tau_gtau, (np.size(tau),2))
    np.savetxt( filename, tau_gtau)

for i in range(0, Usteps+1):
    filename = FileNamePrefix + "_self-energy_U=" + str(U_min+i*
       U_step)
    w_siw = np.array( (w[0].real,U_list_siw[i].imag) )
    w_siw = np.reshape( w_siw, (2*np.size(w[0])), order='F')
    w_siw = np.reshape( w_siw, (np.size(w[0]),2))
    np.savetxt( filename, w_siw)

#pl.figure(1)
#for i in range(0, Usteps+1):
#    pl.plot( w[0] , U_list_gloc[i].imag, label="U= " +str(U_min+ i*
   U_step) )
#pl.xlabel("$i\omega_n$")
#pl.ylabel("$Gloc_(i\omega)$")
#pl.legend()
#pl.title( "Local Green's function")

pl.figure(2)
for i in range(0, Usteps+1):
    pl.plot( w[0] , U_list_siw[i].imag, label="U= " +str(U_min+ i*
       U_step) )
pl.xlabel("$i\omega_n$")
pl.ylabel("$\Sigma_(i\omega)$")
pl.legend()
pl.title( "self energy")

#pl.figure(3)
#for i in range(0, Usteps+1):
#    pl.plot( w[0] , U_list_giw[i].imag, label="U= " +str(U_min+ i*
   U_step) )
#pl.xlabel("$i\omega_n$")
#pl.ylabel("$G0_(i\omega)$")
#pl.legend()
#pl.title( "Bare Green's function")

#pl.figure(4)
#for i in range(0, Usteps+1):
```

```
#    pl.plot( w[0] , U_list_fiw[i].imag, label="U= " +str(U_min+ i*
    U_step) )
#pl.xlabel("$i\omega_n$")
#pl.ylabel("$\Delta_(i\omega)$")
#pl.legend()
#pl.title( "Hybridization")

pl.figure(5)
for i in range(0, Usteps+1):
    pl.plot( tau , U_list_gtau[i].real, label="U= " +str(U_min+ i*
       U_step) )
pl.xlabel("tau")
pl.ylabel("G_(tau)")
pl.legend()
pl.title( "G_(tau)")

#tikz_save( 'siw.tikz' )
pl.show()

############################################################
```

A.2 w2dynamics class FKBetheLattice

```
class FKBetheLattice(BetheLattice):
    """This class implements a bethe lattice with self-consistency in
        matsubaras, with spin resolved
    band-widths. Input: e.g. half-bandwidth= 1, 2 ; Nd = 1. Thus, in
       the limit the Falikov Kimball
    model can be reproduced. """

    def __init__(self, cfg,comm=None):
        BWDefinedLattice.__init__(self, cfg,comm)
        self.use_analytic = False

    def sfw2gfw(self):
        for ineq in self.ineq_atoms:
            if self.magnetism == 'antiferro':
                sfw_slice = slice(None, None, -1)
            else:
                sfw_slice = slice(None)
            zeta = (1j*self.w[np.newaxis,np.newaxis,:] + self.mu -
               ineq.hmean[...,np.newaxis] - ineq.sfw[...,sfw_slice])
            #zeta = 1j*zeta.imag
            dspin2 = np.reshape( ineq.d, (ineq.nd,2), order='C' )
               [:,:,np.newaxis]**2
            ineq.gfw = 2*zeta/dspin2 * (1 - np.sqrt(1 - dspin2/zeta
               **2))

    def giw2siw(self, ineq, giw, gsigmaiw=None):
        BWDefinedLattice.giw2siw(self, ineq, giw, gsigmaiw)
        if self.use_analytic:
            # The analytic formula requires storage of giw
```

```
            ineq.giw = giw
        if self.magnetism == 'para':
            # Similar to the self-energy, when using the analytic
                version of the
            # Bethe self-consistency and wants to force paramagnetic
                solutions,
            # one has to do this.
            ineq.giw[...] = ineq.giw.mean(axis=1)[:,np.newaxis,:]
        ineq.siw = 0.5*ineq.cfg["Udd"] + 1j*ineq.siw.imag

    def gfw2fiw(self):
        """Since we know how to analytically go from an impurity
            greens function to a
        hyb function we only do the calculation of the greens
            function if we do not have a
        g_imp yet.
        """
        for ineq in self.ineq_atoms:
            if self.use_analytic:
                try:
                    if self.magnetism == 'antiferro':
                        giw_slice = slice(None)
                    else:
                        giw_slice = slice(None, None, -1) # inverse
                            because "hole"

                    dspin = np.reshape( ineq.d, (ineq.nd,2), order='C
                        ' )
                    ineq.fiw[...]=(0.25*dspin[:,:,np.newaxis]**2*
                                ineq.giw[...,giw_slice])
                    print >> sys.stderr, " Using analytic formula for
                        self-consistency"
                    return
                except Exception,e:
                    print >> sys.stderr, " Failed to use analytic
                        formula:", e

        print >> sys.stderr, " Using lattice Green's function for
            self-consistency"
        Lattice.gfw2fiw(self)

    def set_fmom(self):
        for ineq in self.ineq_atoms:
            ineq.fmom=-np.reshape( ineq.d, (ineq.nd,2), order='C' )
                **2/4.

    #TODO: def set_fmom(self, ineq):

    def set_crystalfield(self):
            for ineq in self.ineq_atoms:
                if ineq.cfg["crystalfield"]:
```

```
                    ineq.hkmean[:ineq.nd,:]=np.asarray(ineq.cfg["
                        crystalfield"])[:ineq.nd,np.newaxis]
    def set_hkmean(self):
        pass

    def init_matrices(self):
        Lattice.init_matrices(self)
        for ineq in self.ineq_atoms:
            ineq.d = np.array([float(x) for x in self.cfg["General"][
                "half-bandwidth"]])
            dspin = np.reshape( ineq.d, (ineq.nd,2), order='C' )

    def fiw2ftau(self):
        """Transforms the hybridization function from Matsubaras to
            tau using a model"""
        for ineq in self.ineq_atoms:
            dfiw = ineq.fiw[:,:,:] - ineq.fmom[:ineq.nd,:,np.newaxis
                ]/(self.w[np.newaxis,np.newaxis,:]*1j)
            ineq.ftau=(tf.transform(tf.mat2tau(self.beta, 'fermi',
                self.w.size, self.cfg["QMC"]["Nftau"]), dfiw)
                            - ineq.fmom[:ineq.nd,:,np.newaxis]/2.)
            # dirty hack
            ineq.ftau=np.where(ineq.ftau < 0, -ineq.ftau, ineq.ftau).
                real
            # symmetries ftau
            ineq.ftau= 0.5*(ineq.ftau+ineq.ftau[...,::-1])
```

A.3 eval.py

```
def zfact(iw,siw,iw_val=0.):
    """Find gamma and alpha of self energy siw defined on axis iw;

        iw ... real valued numpy array containing grid on pos
            frequency axis
        siw ... complex valued numpy array containing self-energy

    """
    closest = 0.5*len(iw)
    alpha = ((siw.imag[closest+1]-siw.imag[closest])/(iw[closest+1]-
        iw[closest]))
    gamma = siw.imag[closest]- alpha*iw[closest]
    return (gamma,alpha)
```

Bibliography

H. A. Bethe. Statistical theory of superlattices. *Proceedings of the Royal Society of London A: Mathematical, Physical and Engineering Sciences*, 150(871):552–575, 1935.

Nils Bluemer. *Mott-Hubbard Metal-Insulator Transition and Optical Conductivity in High Dimensions*. University Augsburg, 2000.

Ling Chen, B.A. Jones, and J. K. Freericks. Charge-density-wave order parameter of the falikov-kimball model in infinite dimensions. *Phys. Rev.*, B 68, 2003.

Piers Coleman. *Introduction to Many-Body Physics*. Rutgers University, New Jersey, 2015.

J. K. Freericks and V. Zlatić. Exact dynamical mean-field theory of the falicov-kimball model. *Reviews of Modern Physics*, 75:1333–1379, 2003.

Antoine Georges, Gabriel Kotliar, Werner Krauth, and Marcelo J. Rozenberg. Dynamical mean-field theory of strongly correlated fermion systems and the limit of infinite dimensions. *Reviews of Modern Physics*, 68:17–19, 1996.

Benedikt Hartl. *Maximum Entropy Method for Quantum Monte Carlo Simulations*. TU Wien, 2015.

Based on the lecture given by Profs. J. Burgdörfer and Lemell. *StatPhys*. TU Wien, 2011.

Tin Ribic. *Vertex extensions of the dynamical mean field theory for the Falicov-Kimball model*. Masterthesis, TU Wien, 2015.

wikimedia. https://commons.wikimedia.org/wiki/file:bethe_lattice.png, 03 2015.

Alexandre Zagoskin. *Quantum Theory of Many-Body Systems: Techniques and Applications*. Springer, 1998.